NASA TECHNICAL MEMORANDUM

NASA TM X-71768

NASA TM X-71768

INTERIM PREDICTION METHOD FOR EXTERNALLY BLOWN FLAP NOISE

by Robert G. Dorsch, Bruce J. Clark, and Meyer Reshotko
Lewis Research Center
Cleveland, Ohio 44135

1. Report No. NASA TM X-71768	2. Government Accession No.	3. Recipient's Catalog No.
4. Title and Subtitle INTERIM PREDICTION METHOD FOR EXTERNALLY BLOWN FLAP NOISE		5. Report Date 6. Performing Organization Code
7. Author(s) Robert G. Dorsch, Bruce J. Clark, and Meyer Reshotko		8. Performing Organization Report No. E-8423
9. Performing Organization Name and Address Lewis Research Center National Aeronautics and Space Administration Cleveland, Ohio 44135		10. Work Unit No. 11. Contract or Grant No. 13. Type of Report and Period Covered Technical Memorandum
12. Sponsoring Agency Name and Address National Aeronautics and Space Administration Washington, D.C. 20546		14. Sponsoring Agency Code
15. Supplementary Notes		

16. Abstract

An interim procedure for predicting externally blown flap noise spectra anywhere below a powered lift aircraft is presented. Both engine-under-the-wing and engine-over-the-wing EBF systems are included. The method uses data correlations for the overall sound pressure level based on nozzle exit area and exhaust velocity along with OASPL directivity curves and normalized one-third-octave spectra. Aircraft motion effects are included by taking into account the relative motion of the source with respect to the observer and the relative velocity effects on source strength.

17. Key Words (Suggested by Author(s))	18. Distribution Statement Unclassified - unlimited		
19. Security Classif. (of this report) Unclassified	20. Security Classif. (of this page) Unclassified	21. No. of Pages	22. Price*

* For sale by the National Technical Information Service, Springfield, Virginia 22151

INTERIM PREDICTION METHOD FOR EXTERNALLY BLOWN FLAP NOISE

by Robert G. Dorsch, Bruce J. Clark, and Meyer Reshotko

Lewis Research Center

E-8423

SUMMARY

An interim procedure for predicting externally blown flap noise spectra anywhere below a powered lift aircraft is presented. Both engine-under-the-wing and engine-over-the-wing EBF systems are included. This prediction procedure is developed in support of the NASA Aircraft Noise Prediction Program. The method uses data correlations for the overall sound pressure level based on nozzle exit area and exhaust velocity along with OASPL directivity curves and standard normalized one-third-octave spectra.

Aircraft motion effects take into account both the relative motion of the dipole source with respect to the observer and the relative velocity effects on source strength.

The procedure is developed for angles from the engine inlet for which the intense low-frequency dipole noise field dominates. Until a separate analysis is available for the quadrupole-dominated region of the noise field, this region is treated as if it were dipole noise.

The areas of weakness in the prediction method are discussed and recommendations for needed research and development activity in the flap noise area are made.

INTRODUCTION

Short-haul and STOL aircraft employing powered lift systems generate flap interaction noise, which is an additional noise source that must be included in any noise prediction program. This report will provide a method of predicting the flap interaction noise for

powered lift systems using externally blown flaps (EBF). Both engine-under-the-wing (UTW) and engine-over-the-wing (OTW) EBF systems will be included.

The prediction method is presented in response to the need for predicting externally blown flap noise as a component of total aircraft noise for the NASA Aircraft Noise Prediction Program (ANOPP). This Program is located at Langley Research Center and is being developed jointly by various NASA Centers with help from industry representatives. In the Program, the various contributors to and modifiers of aircraft noise are summed at various ground locations in order to predict a noise footprint for single- or multiple-event aircraft flights. The need for the ANOPP requires that this prediction method be based on the present state-of-the-art. Refined techniques and additional data when available will permit up-dating this prediction method.

The externally blown flap (EBF) is recognized as one of the simpler ways to achieve powered lift (e.g., refs. 1 to 3). Unfortunately, a considerable amount of noise is produced by the interaction of the engine exhaust with the surfaces of the flap system (refs. 4 and 5). In fact, with UTW EBF systems the flap interaction noise is the dominant aircraft noise source when highly-noise-suppressed turbofan engines are employed (ref. 5).

Stimulated in part by the Quiet Clean Short-Haul Experimental Engine (QCSEE) demonstration engine program and what was the Quiet Experimental Short Take-Off and Landing (QUESTOL) demonstration aircraft program, extensive inhouse and contractual research and development activity was initiated in the area of powered-lift acoustics during the past five years by the National Aeronautics and Space Administration. The research objectives were to measure, define, and predict the flap noise field for a variety of EBF configurations and to provide insight into flap noise source mechanisms (refs. 5 to 19). These efforts were accompanied by special tests and programs aimed at suppressing flap noise (refs. 20 to 26).

Initially most of the research and development effort was directed towards the UTW system because such an aircraft could more readily

be evolved from current conventional commercial (CTOL) aircraft. However as the magnitude of the flap noise problem became more clearly understood, there was increased emphasis on determining the acoustic characteristics of OTW EBF systems (refs. 14 and 27 to 36). The OTW system takes advantage of the high frequency acoustic shielding provided by the wing and flap system and therefore offers promise of reducing the flap noise perceived below an aircraft.

The development of prediction methods for UTW and OTW flap noise (e.g., refs. 18, 37, 38) has been hampered by a lack of clear understanding and quantitative evaluations of the noise source mechanisms (refs. 14 to 20 and 39 to 50). Among the many flap noise source mechanisms thought to contribute to the UTW noise field are: (1) flap leading edge noise caused by incident turbulence in the exhaust jet; (2) scrubbing noise generated by turbulence produced in the jet-mixing region and convected along the surfaces of the wing and flaps; (3) noise from separated flow on the flaps; (4) trailing-edge noise caused by turbulent eddies and/or shed vortices as they pass the trailing edge of the flap; and (5) jet-mixing noise originating in the distorted and deflected exhaust jet. To complicate matters, different sources may dominate at different angles from the engine inlet and at different velocities (refs. 16 and 19).

With the OTW configuration the noise sources (ref. 14) appear to be similar to the UTW sources with several important differences. First, there is no flap leading edge noise source, as the flap slots are normally covered. In some cases, exhaust flow deflectors may be used to facilitate flow attachment to the wing-flap system (e.g., ref. 30). The presence of a flow deflector introduces an additional broadband source of noise (similar to UTW flap noise) above the wing. Finally, as mentioned previously, shielding of the high frequency components of the jet mixing and surface interaction noise by the wing-flap system tends to give a favorable effect below the aircraft.

In view of the current state of the theoretical and analytical work

in this area, the philosophy used in the prediction procedure of this report will be to assume that for the UTW system the various surface noise sources (mechanisms (1) through (4)) can be lumped together and treated as a dipole field radiating from the trailing flap. The OTW system will be treated in a similar manner.

The prediction procedure which will be developed applies (strictly speaking) to angles from the engine inlet for which the intense low-frequency dipole field dominates. In this region the flap noise varies as the 6th power of the jet velocity. For angles close to the trailing flap direction (at which the jet-mixing noise of the deflected exhaust jet makes an important contribution to the noise), a separate prediction analysis is needed since this source (mechanism (5)) generally has an 8th power dependence on velocity. However, for this interim method, noise at these angles will be treated as though the dipole noise was dominant. This simplification, of course, causes the prediction procedure to become increasingly inaccurate at these angles as the nozzle exhaust velocity is increased. For this reason, in the prediction procedure the maximum effective exhaust velocity (defined later) will be limited to 274 m/s (900 ft/sec).

The prediction procedure makes use of the geometric relationships shown in figure 1 to relate the observation point and the flap noise source on the aircraft. The aircraft is considered the origin, and observation point is at distance R, polar angle θ, and azimuthal angle φ in a plane perpendicular to the engine axis. The flap noise field is described in terms of angle θ_F, which is the projection of angle θ onto the flyover plane, and angle φ.

The approach used for both the UTW and OTW static (stationary aircraft) flap noise predictions will be to calculate the overall sound pressure level (OASPL) at any point (defined by R, θ, and φ in fig. 1) from data correlations and OASPL directivity curves. The one-third octave sound pressure level spectra will then be determined for the given angle from standard flap noise spectra normalized with respect to OASPL. A single spectral shape based on data for the angle yielding the flyover maximum in each case will be used to rep-

resent all spectra in the flyover plane ($\varphi = 0$ in fig. 1). A single spectral shape will also be defined for the wing-tip sideline position, $\varphi = 90^{\circ}$, $\theta = 90^{\circ}$. For azimuthal angles between $\varphi = 0$ and $\varphi = 90^{\circ}$ the spectral shape will be determined by interpolation procedures.

Aircraft motion effects on the static spectra will be taken into account in a separate procedure by approximate empirical and analytical expressions to correct the sound pressure level and frequency for relative airspeed and Doppler effects.

The prediction procedures developed herein apply to EBF systems with effective exhaust velocities of 107 to 274 meters per second (350 to 900 ft/sec).

ANALYTICAL BASIS FOR PREDICTION METHODS

For the UTW EBF system the present state of the art is such that flap noise predictions can in principle be based on analyses and data correlations using nozzle exhaust flow parameters evaluated either at the flap impingement station or at the nozzle exit. For the OTW EBF system only the nozzle exit parameter approach has been sufficiently developed to use in a prediction procedure.

Impingement Parameter Approach, UTW Systems Only

In order to obtain a basis for analyzing and correlating the UTW test data available, it is necessary to make some simplifying generalizations about the sources of the flap noise. UTW blown flap interaction noise typically has a radiation pattern (see figs. XII-4 and XII-8 of ref. 14) having two rather flat peaks located in the flyover plane between 50° and 80° to each side of the deflected exhaust flow direction (defined approximately by the trailing flap chordline). Following the general analytical approach of Curle (ref. 42), it will be assumed that this noise results from two principal components. One is a strong quadrupole noise emanating from the nozzle exhaust shear layer and particularly from the deflected and distorted exhaust fluid flowing adjacent to the flaps (refs. 15, 43, and 44). This tur-

bulent mixing noise is intensified as well as reflected by the presence of solid surfaces in the exhaust flow. This quadrupole source has a directivity which peaks (at least for cold exhaust flows) at an angle of about 20° to 30° with respect to the deflected exhaust flow direction (similar to the data of ref. 15). The other noise source is an intense dipole noise originating at the flap surfaces (refs. 39 to 42). This source has a radiation pattern which peaks at approximately a 90° angle with respect to the deflected flap chordline direction. The overall sound pressure level will therefore show an exhaust velocity dependence between V^8 (quadrupole) and V^6 (dipole), depending on the angle θ and on the magnitude of the velocity.

The dipole noise is dominant in the forward quadrant ($\theta = 0^{\circ}$ to $\theta = 90^{\circ}$) below the wing of a blown flap system, and because of its high intensity, usually dominates the peak flyover noise. In this region it will be assumed (see refs. 40 and 16) that the RMS acoustic pressure, p, for the low frequency portion of the flap noise spectrum can be represented by

$$p^2 \sim \left(\frac{\rho_a}{RC_a}\right)^2 \int_A I_i^2 V_i^6 \, dA \qquad (1)$$

where the integral is based on the radial profiles of the jet impingement velocity, V_i, and the inflow turbulence intensity, I_i, at the flap axial station. (All symbols are defined in the appendix.) The integral form of equation (1) results from taking into account the strong velocity and turbulence gradients present in the jet exhaust plume (in contrast to an airfoil immersed in a uniform flow field). Inasmuch as flap noise spectra peak at low frequency, the overall sound pressure level (CASPL) can be represented by equation (1) with good accuracy. It was assumed in deriving equation (1) that the flap noise is independent of the exhaust plume temperature. The effect of temperature has not been established at this time but is thought to be small in the velocity range of interest. This assumption allows the density

term to be taken outside the integral in equation (1).

For EBF systems having similar radial turbulence intensity profiles and similar impingement velocity profiles at the flap impingement station, the integral of equation (1) can be approximated for scaling purposes by the technique used in references 15 to 16 to give the simplified relation

$$p^2 \sim \left(\frac{\rho_a}{RC_a}\right)^2 A_i V_{i,p}^6 \tag{2}$$

where $A_i = (\pi/4)d_i^2$ and $V_{i,p}$ is the peak impingement velocity (ref. 21) obtained from the nozzle exhaust velocity profile at the flap station. The characteristic impingement diameter, d_i, is arbitrarily taken for scaling purposes as the width of the profile at the flap station where the velocity is 80 percent of the peak impingement velocity. Both $V_{i,p}$ and d_i are obtained from nozzle exhaust velocity radial profiles measured without the presence of the wing and flap system. The velocity profiles are calculated (assuming fully expanded flow) from total pressure rake data.

The advantages of using flap impingement parameters to correlate flap noise data are illustrated in figures 2 and 3. Normalized overall sound pressure level, OASPL - 10 log $[(A_i/A_o)(R_o/R)^2]$, for 2-flap EBF configurations is plotted in figure 2 as a function of the dimensionless peak impingement velocity, $V_{i,p}/V_o$. The data points (from ref. 7, 16, and 24) are for single-stream nozzles (conical, plug, 5:1 slot, 8-tube mixer, and 7-lobe mixer), with 60^o trailing flap position, and for directivity angles corresponding to the radial peak OASPL value. The small-scale 5:1 slot nozzle and 8-tube mixer configuration data are from unpublished Lewis Research Center tests. The small-scale data were measured at 3.05 m (10 ft) radius, whereas the large cold-flow model data were taken at 15.24 m (50 ft). It should be noted that the OASPL in figure 2 is normalized using the dimensionless impingement area, A_i/A_o. Figure 2 shows that the

parameters A_i and $V_{i,p}$ correlate the two-flap single-stream nozzle EBF data very well. Further, the data are fitted by a 6th power of velocity curve. Thus, the use of impingement parameters in the velocity correlation gives very good agreement with the simple dipole source model (eq. (2)). Further, EBF configurations having both high decay (5:1 slot, 8-tube mixer, and 7-lobe mixer) and low decay (conical and coaxial) exhaust nozzles are correlated by a single set of parameters.

The same impingement parameters are used for coaxial nozzle configurations in figure 3 (taken from ref. 16) where the flap noise data from turbofan engine tests are compared with data from cold-flow model tests. Both models are three-flap systems. The normalized OASPL is shown as a function of $V_{i,p}$ in figure 3(a) for the angle θ_F yielding the flyover-track maximum in each case. The flap noise directivity patterns are compared at two values of peak impingement velocity in figure 3(b). Figure 3 again shows that good data correlations can be achieved in terms of flap impingement parameters.

In spite of the good correlations shown in figures 2 and 3, the use of flap impingement parameters A_i and $V_{i,p}$ to correlate flap noise data is not completely free of problems nor is it a fully developed concept. Detailed exhaust velocity profile data or complete correlations which give both $V_{i,p}$ and d_i are not always available for making comparisons and/or predictions of flap noise. This is particularly true in design or parametric studies involving "paper" engines. In addition, the role of inflow turbulence intensity (eq. (1)) needs further study. Two-stream coaxial nozzles and single-stream nozzles tend to have dissimilar radial turbulence intensity profiles at the flap station. It was shown in reference 16 that a third exhaust-flow impingement parameter related to turbulence intensity (or turbulent mixing) was required to correlate data from cold-flow single-stream nozzle EBF configurations with data from cold-flow model configurations having two-stream coaxial nozzles. Further, the use of d_i for the length scale in the Strouhal relation when correlating flap noise spectra (ref. 16) requires further study and verification. Thus, in view of the current incomplete state of development of the impingement parameter approach,

it is often necessary to compare data and/or make predictions using nozzle exit exhaust velocity and exit area as parameters.

Nozzle Exit Parameter Approach

UTW EBF systems. - For configurations having exhaust nozzles with low velocity decay (nonmixer type) or nozzles with similar decay characteristics, flap noise data can be compared by using an effective nozzle exhaust velocity, V_E, and total exhaust nozzle area, A_T. The effective exhaust velocity is obtained by evaluating the velocity profile integral of equation (1) at the nozzle exhaust exit planes (instead of at the flap station). This approach amounts to the approximation that

$$A_T V_E^6 \sim A_i V_{i,p}^6 \tag{3}$$

or in terms of RMS acoustic pressure

$$p^2 \sim \left(\frac{\rho_a}{RC_a}\right)^2 A_T V_E^6 \tag{4}$$

where, for a two-stream nozzle

$$V_E = \left(\frac{A_C V_C^6 + A_F V_F^6}{A_T}\right)^{1/6} \tag{5}$$

For single conical (round convergent) nozzles, $V_E = V_N$ where V_N is the nozzle exhaust velocity, and A_T simply becomes, A_N, the nozzle exit area. Equation (5) was used in the simplified flap noise prediction method of reference 18. The use of equations (4) and (5) assumes that the velocity decay and spreading characteristics of the EBF system which are being correlated are comparable and that the differences that do exist will have only a secondary effect on the flap noise.

Examples of flap noise data correlated in terms of nozzle exit parameters are shown in figures 4 to 6. Data for four 2-flap configurations plus a swept-wing 2-flap configuration are shown in figure 4 (adapted from ref. 16). Normalized overall sound pressure levels measured at the angle corresponding to the radial peak value for each configuration are plotted against normalized effective nozzle exhaust velocity. These OASPL data are for the angles corresponding to the radial peak in each case, where the dipole noise component of the flap noise should be strongest. The data correlation in terms of A_T and V_E is good. However, even at these angles where the dipole noise should be dominant, the OASPL varies with the 6.7 power instead of the theoretical 6th power of the effective nozzle exhaust velocity. This exponent of 6.7 was also noted in reference 16.

Turbofan engine and cold-flow model coaxial-nozzle EBF test results for landing flap angle settings are shown in figure 5 (adapted from ref. 16). The normalized OASPL is plotted against V_E/V_o for the angles corresponding to the flyover maximum. With the exception of the data point for the lowest-velocity (low fan speed) engine test, the data are also correlated by about the 6.7 power of effective nozzle exhaust velocity.

Flap noise spectra for the cold-flow coaxial-nozzle model and turbofan engine tests were also compared in reference 16 and are reproduced in figure 6. Normalized SPL spectral density (SPL - OASPL + 10 log V_E/D_T - 10 log Δf) curves derived from one-third octave SPL data for the angle yielding the flyover maximum in each test are plotted against a Strouhal number ($f D_T/V_E$) based on nozzle exit parameters. The engine data are for a 55^o trailing flap angle position, and the cold-flow 3-flap coaxial-nozzle model data are for a 60^o position. The engine data are for a θ_F of 80^o and the cold-flow model data are for a θ_F of 0^o. Both sets of one-third octave SPL data were corrected for ground effects. Figure 6 shows that the spectral shapes are very similar and that the spectra

for the coaxial nozzle EBF configurations can be correlated in terms of exit parameters.

OTW EBF systems. - Noise levels for OTW EBF systems are strongly influenced by shielding. Although considerable noise may be generated by the deflector (used to spread the flow and promote attachment of the flow to the upper wing and flap surface), this added noise may have only a minor effect on noise levels below the wing. Noise source levels (without shielding effects) can be compared on the basis of power spectra (PWL), so that energy radiated above the wing as well as below the wing is included in the spectra.

Typical sound power level spectra for models of two types of OTW EBF systems are shown in figure 7. Spectra for the conical nozzle with deflector configuration are shown in figure 7(a). Figure 7(b) shows spectra for a configuration having a 10:1 slot nozzle canted towards the wing to promote attachment. For both OTW configurations there is a large increase in low frequency noise compared to the nozzle alone. This low frequency noise is thought to be primarily caused by trailing-edge-dipole noise (ref. 40) although the exact nature of this source is not known at this time. When the flow deflector is used (fig. 7(a)) to promote flow attachment there is a large increase in the noise generated at middle and high frequencies.

Typical SPL spectra below the aircraft (fig. 8) show that the wing shields much of the high frequency noise generated by the deflector. Because of this wing shielding it was shown in reference 30 that the spectral shape for angles below the aircraft is less sensitive to the type of nozzle system employed than would be suggested by the power spectra of figure 7. However, this is not the case at the wing-tip sideline position where the wing cannot shield the middle and high frequency noise from the observer. Thus, the nozzle configuration, including any flow attachment devices, must be specified.

For the OTW prediction procedure of this report the reference configuration has a conical nozzle with deflector. Inasmuch as deflector noise has many similiarities with OTW flap noise, it will be assumed that both the low frequency trailing edge noise and the de-

flector noise can be represented by dipole noise fields with a 6th power of velocity dependence. Further, inasmuch as the nozzle is generally in close proximity to the deflector and wing, it will be assumed that exhaust velocity decay does not play an important role. Under these conditions one would expect that the OASPL for observer angles below the wing would vary as the 6th power of exhaust nozzle exit velocity. This was shown to be true in reference 32. Figure 9 (adapted from ref. 32) shows the variation of OASPL with exhaust velocity measured at $\theta_F = 90^o$ for a large cold-flow OTW EBF model. The 6th power of velocity curves indicated in the figure fit the data quite well.

Based on the preceding assumptions, the RMS acoustic pressure, p, for OTW flap noise can be represented by the relation

$$p^2 \sim \left(\frac{\rho_a}{RC_a}\right)^2 A_N V_N^6 \tag{6}$$

where A_N and V_N are the nozzle exit area and exhaust velocity. For OTW fan-jet engines the two exhaust systems are normally mixed with an internal mixer so that V_N must be replaced with an effective mixed velocity V_E, and A_N is the mixed-exhaust exit area A_T.

FLAP NOISE PREDICTION METHODS

Several flap noise prediction methods are currently available in the open literature. Two of the more complete methods which have been programmed for computers are given in references 37 and 38.

In reference 37 both hand calculation procedures and computer programs for predicting EBF noise are given for UTW and OTW configurations. Both prediction methods are based on the nozzle exit parameter approach and are for stationary aircraft. The procedures start with the calculation of Total Power Level (PWL_T) from the specified nozzle exhaust velocity and nozzle exit area. The use of PWL_T as the starting reference noise level offers the advantage that relatively simple theoretical expressions can be employed for the

various flap noise sources (e.g. scrubbing noise). However, PWL_T is very difficult to measure experimentally because of the strong three-dimensional nature of the flap noise field. Further, for the OTW system the largest contribution to the total power level comes from the region above the wing (especially if a flow deflector is used) whereas the region of interest is below the wing.

The method of reference 38 uses a partial-impingement-parameter approach to predict UTW flap noise. Flap impingement velocity is used as the velocity parameter. However, the scale parameter employed is nozzle exit area. Overall sound pressure level (OASPL) at one meter is calculated from these parameters and is used as the starting point in determining the flap noise levels. Flight effects are included as an intrinsic part of the prediction procedure. An assumed correction factor for jet temperature is also included. The prediction procedure is based on the small-scale conical-nozzle EBF model acoustic data of reference 7. For the reference configuration the flap impingement (dipole) noise is assumed to dominate over the mixing-noise of the deflected jet. Strictly speaking, the flap noise prediction method given in reference 38 does not apply to EBF systems having separate-flow coaxial nozzles as the acoustic and exhaust velocity decay relations given are based on single-stream conical nozzle data. Further, although impingement velocity is used as a parameter, the prediction procedure in its present form does not apply to EBF systems having mixer-decayer nozzles. The nozzles have a high rate of exhaust velocity decay accompanied by a considerable amount of jet spreading and in addition may have complex multi-peaked radial velocity profiles at the flap station (e.g., ref. 21).

A simplified flap noise prediction method for particular UTW and OTW EBF powered lift systems assumed to have high-bypass ratio engines in the 25 000-lb thrust class is presented in reference 18. Data from the tests reported in references 6, 12, and 32 were used for the data base. Spectral data were smoothed to remove cancellations and reinforcements due to ground reflections. However, the data used were not corrected to free field conditions. Nozzle exit

parameters were used to correlate the data. The starting point in the procedure is the calculation of the reference OASPL (at distance R and $\theta_F = 90^o$) from the nozzle exit parameters. Aircraft motion is not taken into account. The flap noise prediction method of reference 18 has limited application since the spectra given apply directly only to a particular size EBF system.

RECOMMENDED INTERIM PREDICTION PROCEDURE

Approach

The recommended interim prediction procedure for flap noise will be based on the nozzle exit parameter approach of reference 18 for both the UTW and OTW EBF systems. As in reference 18 the flap noise levels will be based on data correlations of the overall sound pressure level in a selected reference direction in terms of nozzle exit flow parameters. In contrast to reference 18, however, both the OASPL and the normalized spectra will be corrected to free field conditions. In addition, a larger data base (including the results of ref. 16) will be employed.

The recommended interim prediction procedure will be for stationary aircraft. Aircraft motion effects on the predicted static flap noise field are treated in a separate section of this report. The procedure for predicting aircraft motion effects has been separated from the static prediction procedure because of the greater degree of uncertainty in this area. This allows the user the option of either including or omitting flight effects and also permits separate updating and improvements of each section in the future.

Because the procedure is based on nozzle exit parameters the interim prediction method will apply directly only to EBF systems having conventional low decay exhaust nozzles.

Reference UTW and OTW configurations. - The curves and equations to be presented in the flap noise prediction procedure are based on data for specific UTW and OTW configurations. These configurations were the baseline configurations in NASA-Lewis test

programs and are shown in figure 10 and 11. The cold-flow UTW and OTW test configurations were roughly one-half scale models of the corresponding turbofan engine test configurations. The baseline UTW configurations are shown in figure 10 and the corresponding OTW test configurations are shown in figure 11. The predictions made herein are valid for these specific configurations. The sensitivity to certain changes in nozzle and flap geometry is discussed as part of the procedure.

Region of application. - As was stated earlier, UTW flap noise is typically dipole-noise-dominated at right angles to the deflected flow direction, and tends to be quadrupole-noise-dominated in the region near the deflected flow direction. The noise level and spectrum predictions of this method are at present developed principally for the dipole-dominated region ($0^{\circ} \leq \theta_F \leq 150^{\circ} - \psi$). When an analysis of the data for the quadrupole-dominated region becomes available, this region can then be treated as a separate and distinct noise source (similar to the approach used in reference 37) with its own level, directivity, and spectrum predictions. Total flap noise will be the sum of the noise from the dipole and quadrupole sources. Until this has been accomplished, predictions for the quadrupole-dominated region ($150^{\circ} - \psi \leq \theta_F \leq 180^{\circ}$) will be approximated as an extension of the dipole-dominated region. The OASPL predicted for the dipole sources will be applied to this quadrupole-dominated region, modified by the the measured values of directivity. Spectra for the quadrupole-dominated region will be approximated at present by the spectra developed for the dipole-dominated region.

Coordinate system. - The position of any observer, point 0 of figure 1, is described by the coordinates R, θ, and φ in a reference coordinate system moving with the aircraft. The polar angle θ is the angle between the engine inlet axis and the position vector R of the observer. The azimuthal angle φ lies in a plane perpendicular to the engine axis. A large fraction of the available flap noise data have been measured in the flyover plane ($\varphi = 0$) shown in figure 1. Most of the remaining data were measured in, or close to,

the plane perpendicular to the engine axis ($\theta = 90^{o}$) in order to obtain directivity as a function of the angle φ. Data correlations are therefore available in terms of the angles θ_F and φ. The angle θ_F is the projection of the angle θ onto the flyover plane. The projected angle θ_F is related to the reference coordinate system by

$$\tan \theta_F = \tan \theta \cos \varphi \tag{7}$$

At $\varphi = 90^{o}$, θ_F is indeterminate, so that this relation is restricted to $\varphi < 90^{o}$ (i.e., the aircraft must be in the air). At $\varphi = 90^{o}$ (aircraft on the runway) the noise estimates will have to be made from directivity data for this plane.

Prediction method. - The procedure for calculating the spectrum for a stationary aircraft at any point 0 of figure 1 as developed herein contains a number of steps. The method chosen starts with the calculation of the free-field flap noise OASPL in one direction (the reference direction) by equations involving the distance from the aircraft, the flap angle, the nozzle area, and the effective exhaust velocity. Curves of the three-dimensional OASPL directionality are then presented so that adjustment can be made to the reference OASPL to obtain OASPL levels in other directions below the aircraft.

In the final step of the development, curves are presented for one-third octave SPL spectra which are normalized with respect to OASPL. The normalized spectra relate the SPL spectrum band levels to a Strouhal number based on exhaust nozzle diameter and exhaust velocity.

Correlation parameters. - The overall sound pressure level in the reference direction, $OASPL_{REF}$ is calculated from flap noise data correlated in terms of exhaust nozzle exit parameters. These parameters are the total nozzle exit are, A_T, and the effective exhaust velocity, V_E.

For coaxial flow nozzles with low velocity decay rates and having essentially unmixed flows at the exit, the effective exhaust velocity is expressed by the noise-weighted average given in equation (5) and repeated here.

$$V_E = \left(\frac{A_C V_C^6 + A_F V_F^6}{A_T} \right)^{1/6} \tag{5}$$

The subscripts F and C refer to the fan and core flows, respectively, and the component velocities are the ideal fully expanded velocities at each nozzle exit. The total exhaust area A_T is defined by $A_T = A_C + A_F$.

In the case of an internal mixer-type nozzle a mass-average velocity is used for the effective velocity defined by

$$V_E = \frac{BPR \cdot V_F + V_C}{BPR + 1} \tag{8}$$

where BPR is the mass-flow bypass ratio.

For the correlations used in this report, the range of effective exhaust velocities was between 107 and 274 meters per second (350 and 900 ft/sec).

Data sources. - The curves and equations used in this flap noise prediction procedure are based primarily on data from two sources: TF34 turbofan engine tests conducted by the General Electric Co. under a NASA-Lewis contract (refs. 12 and 13); and large cold-flow model tests at the Lewis Research Center (refs. 6, 16, 30, and 32). Both tests were conducted using under-the-wing (UTW) and over-the-wing (OTW) configurations. Small-scale (2-in. nozzle diam.) cold flow UTW test data reported in references 7 and 8 along with recent three-flap small-model test data taken at Lewis Research Center and at Lockheed-Georgia Company (NASA Contract NAS3-16831) were used as a guide in establishing three dimensional directivity relationships and to help in interpreting the large model and engine test results.

(6)). These quantities in turn are dependent on the ambient temperature and pressure at the time of the sound measurements. The data used for the correlations of this report were therefore normalized to standard day noise source conditions. It should be pointed out that the standard day

normalization procedure was applied to data already corrected to "lossless" by the customary atmospheric attenuation correction procedure. In terms of OASPL the data were converted to standard day conditions by the following relation

$$OASPL_{STD} = OASPL_a + 10 \log\left[\left(\frac{T_a}{T_{STD}}\right)^3 \left(\frac{P_{STD}}{P_a}\right)^2\right] \qquad (9)$$

where T_a and P_a are the ambient temperature and pressure on the day of the test.

The standard day correction was usually less than ±0.6 dB and did not exceed ±1.0 dB. However, it was found that this correction reduced data scatter.

Under-the-Wing Configurations

Reference OASPL. - The reference direction chosen is $\varphi = 0$, $\vartheta = \theta_F = 90^o$ in figure 1 for the determination of the reference overall sound pressure level, $OASPL_{REF}$. Overall sound pressure levels in the region of interest have a 6.7-power dependence on nozzle exhaust velocity and a first-power dependence on nozzle area, as shown in figure 5 and in reference 16. Values of $OASPL_{REF}$ presented have all atmospheric attenuation removed (i.e., lossless) and have been corrected for ground effects to give free field values.

For a point at distance R from the flap system, $OASPL_{REF}$ is given for the UTW configuration by the equation

$$OASPL_{REF} = K + 10 \log\left[\left(\frac{A_T}{A_o}\right)\left(\frac{R_o}{R}\right)^2\right] + 67 \log\left(\frac{V_E}{V_o}\right) \qquad (10)$$

where $OASPL_{REF}$ is the overall sound pressure level in the geometric reference direction ($\theta_F = 90^o$, $\varphi = 0^o$) at the same distance R. The reference quantities A_o, R_o, and V_o are given in the List of Symbols. The parameter K is equal to the overall sound pressure level at the reference conditions.

Although the parameter K (eq. (10)) varies with the flap angle and nozzle position and size with respect to the wing and flaps, for the geometries of figure 10 only the flap angle dependence need be considered. In figure 12 values of K are shown at several flap angles ψ for the UTW configurations shown in figure 10. The K values can be approximated (to within ±1.5 dB) by

$$K = 83.6 + 0.14\psi \tag{11}$$

where ψ is the angle in degrees between the trailing flap and the mean chord line of the wing. This relation is similar to that in reference 18.

Directivity. - The directivity of the UTW flap noise is treated as the sum of two components: (1) the flyover plane ($\varphi = 0$) directivity, $\left(\Delta_{\theta_F}\right)_{\varphi=0}$, shown in figure 13, where

$$\left(\Delta_{\theta_F}\right)_{\varphi=0} = \mathrm{OASPL}_{\theta_F,\,\varphi=0} - \mathrm{OASPL}_{REF} \tag{12}$$

and (2) the azimuthal directivity, $\left(\Delta_{\varphi}\right)_{\theta_F}$ where

$$\left(\Delta_{\varphi}\right)_{\theta_F} = \mathrm{OASPL}_{\varphi,\,\theta_F} - \mathrm{OASPL}_{\varphi=0,\,\theta_F} \tag{13}$$

The $\left(\Delta_{\varphi}\right)_{\theta_F}$ are given by a simple curve fit

$$\left(\Delta_{\varphi}\right)_{\theta_F} = \beta(\cos\varphi - 1) \tag{14}$$

The parameter β is a function of θ_F and the flap angle, ψ. Values of β are given in figure 14.

From the curves of figures 13 and 14 and equation (14), OASPL can be predicted for directions other than the reference direction by the equation

$$\mathrm{OASPL}_{\theta_F,\,\varphi} = \mathrm{OASPL}_{REF} + \left(\Delta_{\theta_F}\right)_{\varphi=0} + \left(\Delta_{\varphi}\right)_{\theta_F} \tag{15}$$

The Δ_{θ_F} curves shown are composites of several sets of data and represent, in the opinion of the authors, the best averages of the data available at this stage with flap noise experiments. The Δ_{φ} values are based primarily on small-scale data trends, with the magnitudes adjusted to be consistent with large-model results. These Δ_{φ} values must therefore be considered very tentative.

In general, the most directivity effect in both θ_F and φ directions occurs with flaps at the high angle (ψ) settings. Jet noise apparently begins to contribute to the θ_F directivity at the higher jet velocities (i.e., above 260 m/sec (850 ft/sec)), causing the noise to shift somewhat from the forward to rear quadrants in θ_F. This effect appears as scatter in the original Δ_{θ_F} data and is omitted in these recommended curves.

As indicated earlier, the Δ_{θ_F} curves are extrapolated into the region dominated by quadrupole noise from the deflected jet. These extrapolations are average values over a range of velocities (107 to 274 m/sec). Under most conditions, the inaccuracy caused by these approximations when calculating flyover or sideline noise levels will not be serious.

Normalized spectra. - Normalized and lossless free field one-third octave spectra (SPL-OASPL) are given as a function of Strouhal number in figure 15 for the UTW configurations of figures 10(a) and (b). The Strouhal number is based on the effective exhaust velocity, V_E, and the equivalent diameter of the nozzle, D_T, calculated from the total exit area A_T. Figure 15(a) gives the spectral shapes in the flyover plane ($\varphi = 0$) for trailing flap angles (ψ) of 20^o, 40^o, and 60^o. The three spectra are based on data measured at the angle yielding the flyover maximum OASPL in each case. However, the shapes of the spectra are quite insensitive to θ_F, so these normalized spectra will be used at all θ_F angles in the flyover plane, even though they apply strictly only for the region in which dipole flap noise is dominant ($0^o \leq \theta_F \leq 150^o - \psi$). For trailing flap angles between those shown in figure 15(a), linear interpolation should be used to determine the spectrum shape.

The normalized spectrum at the wing-tip sideline position ($\theta = 90^o$, $\varphi = 90^o$) is shown in figure 15(b). This spectrum shape is recommended at $\varphi = 90^o$ for all flap deflection angles, ψ, and for all polar angles, θ.

For azimuthal angles between $\varphi = 0$ (fig. 15(a)) and $\varphi = 90^{\circ}$ (fig. 15(b)) a linear interpolation of the spectral shape is recommended.

The normalized, lossless one-third octave sound pressure level spectra of figure 15 can be represented in functional form to facilitate computer calculation by methods detailed in reference 19

Sensitivity to variations to the reference configuration. - If the nozzle relative position and diameter are significantly different from the reference geometries of figures 10(a) and (b) the K values of equations (10) and (11) should be modified. An indication of the sensitivity of K to these differences can be drawn from the tests of references 5 to 14. Generally, noise levels (and K) decrease slowly for nozzle relative displacement in the forward direction ($\theta = 0^{\circ}$). For example, advancing the turbofan engine of reference 13 in the direction $\theta = 0^{\circ}$ by a distance of two-thirds of an equivalent nozzle diameter resulted in 0.9 dB decrease in K. However, limited data at LeRC indicate that when the distance from the nozzle to the flap impingement point is decreased substantially (i.e., to less than 3 diam), the noise level produced may be reduced by several decibels; this effect is probably due to reduction in the size of the highly turbulent region of mixing that strikes the flap surface. Lowering the turbofan engine in the direction $\theta_F = 90^{\circ}$ by 0.24 diameter decreased K by 2 dB. In the cold-flow model tests of reference 16 lowering the conical exhaust nozzle by 0.77 diameter caused a 2-dB decrease at high flap deflection (60° trailing flap). At low flap deflection (20° trailing flap) lowering the nozzle the same amount caused an 8 to 10 dB decrease in noise because more than half of the high velocity region of the jet exhaust did not impinge on the flap system. Thus, lowering the engine causes a modest decrease in noise ($1\frac{1}{2}$ to 2 dB) until the high velocity portion of the jet exhaust begins to miss the flap system. At this point there is a substantial decrease in noise (ref. 16).

Conversely, in tests run with the exhaust nozzle in the normal position but with the flaps highly extended even at low flap angles (ref. 16), it was found that K was relatively insensitive to variation in flap angle. In this case the area on the flaps impinged by the high velocity exhaust did not decrease significantly as the flap setting angle was decreased from large

angles. Hence, the noise level (and K) was relatively insensitive to ψ, decreasing only 0.4 dB as ψ decreased from 60° to 20°. The following relation for K was found to hold:

$$K = 91.4 + 0.01\,\psi \tag{16}$$

Note that when $\psi = 60^{\circ}$ equation (16) gives the same value of K as equation (11).

The parameter K is not very sensitive to changes in the nozzle size relative to the flap size for moderate departures from the reference configuration. For large increase in nozzle size reference 14 indicates that with constant wing and flap size, the OASPL is approximately proportional to $10 \log D$ rather than $10 \log A_T$.

The trends with the geometry changes discussed in this section are based on meager data; therefore a generalized method of obtaining correction factors will not be proposed. Where possible, specific correction factors should be obtained from scale model test data.

Over-the-Wing Configuration

As was the case for UTW configurations, the predictions for OTW configurations apply to the specific configurations shown in figure 11, which were the baseline configurations used in the test programs.

Reference OASPL. - The reference direction is taken to be the same as for the UTW configuration ($\varphi = 0$, $\theta = \theta_F = 90^{\circ}$ in fig. 1). Overall sound pressure ($OASPL_{REF}$) show a sixth-power dependence on nozzle exhaust velocity and a first-power dependence on nozzle exit area as in reference 32. The free-field lossless $OASPL_{REF}$ for a point at distance R from the flap system is given by

$$OASPL_{REF} = K + 10 \log\left[\left(\frac{A_T}{A_o}\right)\left(\frac{R_o}{R}\right)^2\right] + 60 \log\left(\frac{V_E}{V_o}\right) \tag{17}$$

The values of K obtained from experimental data for OTW configurations (refs. 30 and 32) are shown in figure 16 to be approximated within ±1 dB by

$$K = 85.1 + 0.01\,\psi \qquad (18)$$

for flap angles, ψ, between 20^{o} and 60^{o}.

Directivity. - The OTW directivity for OASPL in the θ_F and φ planes is given in figure 17. Three-dimensional directivity data for the OTW configuration is even more sparse than for the UTW configuration. Flyover $\left(\Delta_{\theta_F}\right)$ and azimuthal (Δ_{φ}) directivity factors are defined the same as for UTW, but Δ_{φ} data exists only for θ_F angles near 90^{o}. Until more data becomes available, the azimuthal variation Δ_{φ} with φ is assumed to be the same for all θ_F as at $\theta_F = 90^{o}$. The equation for $OASPL_{\theta,\varphi}$ is

$$OASPL_{\theta_F,\,\varphi} = OASPL_{REF} + \left(\Delta_{\theta_F}\right)_{\varphi=0} + \left(\Delta_{\varphi}\right)_{\theta_F=90^{o}} \qquad (19)$$

In this azimuthal directivity, a minimum occurs in Δ_{φ} between low φ angles, where low frequency trailing edge noise predominates, and $\varphi = 90^{o}$, where the high frequencies above the wing are only partly shielded. The only data available for the Δ_{φ} factor were at a 20^{o} flap angle for the large model tests of reference 32, and 40^{o} flap angle for the turbofan engine tests of reference 32; the curve shown represents an average of these test results. There is considerable spread between the data from the turbofan tests and large model tests, which may be a result of added shielding provided by the relatively longer span of wing used in the large model tests. In the OTW tests with the large model, the ratio of wing span (from nozzle centerline) to nozzle diameter was 8.3; in the turbofan tests the ratio was only 3.1.

As with the UTW directivity curves, the OTW curves for Δ_{θ_F} are extrapolated into the quadrupole noise region as an interim means of predicting noise for angles near the direction of the trailing flap. Also, as in the UTW case, the θ_F directivity in the flyover plane shifts more toward the rear quadrant with increasing exhaust velocity, but this effect is again neglected in the recommended curves.

Normalized spectra. - Normalized and lossless free-field one-third octave spectra (SPL-OASPL) are given in figure 18 as a function of

Strouhal number for the OTW configuration. Figure 18(a) gives the spectral shapes in the flyover plane ($\varphi = 0^{o}$) for trailing flap angles of 20^{o} and 60^{o}. The spectra are based on data measured at the angle yielding the flyover maximum OASPL in each case. The normalized spectra will be used to represent the spectral shape at all θ_F angles in the flyover plane, although as with the UTW spectra, they apply strictly only for the dipole-dominated region (i.e., $0^{o} \leq \theta_F \leq 150^{o} - \psi$). For flap angles, ψ, between 20^{o} and 60^{o} linear interpolation should be used to determine the spectral shape.

The normalized spectrum at the wing-tip sideline position ($\theta = 90^{o}$, $\varphi = 90^{o}$) is shown in figure 18(b). When $\varphi = 90^{o}$ this spectrum shape is used for all flap deflection angles, ψ, and for all polar angles θ.

It is recommended that the flyover spectrum shapes of figure 18(a) be used for φ angles between 0^{o} and 65^{o}. Linearly interpolated shapes should be used from $\varphi = 65^{o}$ to 90^{o}.

Sensitivity to variation in configuration. - As discussed earlier in this report (and in ref. 30) the flap noise spectra below the wing are only moderately sensitive to configuration changes because of the strong effects of wing shielding. However, at the wing-tip sideline station the effects of shielding are negligible so that the nozzle shape and/or type of attachment device used can have a major effect on the spectral shape. Thus, if the prediction procedure of this report is applied to an OTW configuration having a nozzle geometry which is significantly different from the reference configuration, the results would be expected to apply reasonably well below the aircraft but would be increasingly in error at large azimuthal angles, φ.

Experiments have shown (e.g., refs. 14 and 30) that a more important variable is the ratio of shielding length to nozzle diameter (or slot height for a rectangular nozzle). For example, recent OTW tests at the Lewis Research Center have shown that a reduction in the shielding length (distance from the nozzle exit plane to the flap trailing edge) of the reference configuration (fig. 11(b)) by about one-third caused approximately a 5-dB increase in the flap noise level. This is consistent with the small scale results discussed in references 14 and 30.

Calculation Procedure

The relations for $OASPL_{REF}$, directivity curves, and recommended normalized spectrum shapes can be used to construct 1/3-octave SPL spectra for flap noise at an observer point located at distance R in a direction defined by θ and φ for a given EBF system.

The geometrical relationships between an observer position on the ground and the aircraft position and attitude at some instant in time must first be solved to determine the observer position in R, θ, and φ with respect to the aircraft as defined in figure 1. From the engine size and type, the proper values of areas and velocities must be chosen to calculate an effective velocity, total exit area, and equivalent diameter of the nozzle. For an UTW or OTW configuration, K is then calculated for the correct flap angle from equation (11) or (18), and $OASPL_{REF}$ is calculated by equation (10) or (17) for the distance R. The appropriate directivity factors in Δ_{θ_F} and Δ_{φ} are applied as in equation (15) or (19) to find the OASPL at the observer location (R, θ, φ). Next, the appropriate normalized spectrum, with interpolation as directed, is selected for the observer angular coordinates θ and φ. The Strouhal number for each 1/3-octave band center-frequency is then calculated using the effective exhaust velocity and nozzle equivalent diameter. For each 1/3-octave band center frequency the SPL is then determined from the selected normalized spectrum by using the corresponding Strouhal number and the OASPL at the observer location. This procedure yields the free-field, lossless 1/3-octave SPL spectrum for the flap noise component at the observer location when the aircraft is at the specified location.

Various corrections must be made to this spectrum. These include the effects of multiple engines, atmospheric attenuation for the distance R, fuselage or engine shielding, and extra ground attenuation. Corrections for small variations from the reference nozzle-wing-flap geometry may also be made, if data are available. Finally, the spectra need to be corrected for the aircraft motion effects discussed in the next section.

Estimates of Accuracy of Prediction Procedure

As pointed out in reference 38 it is "extremely difficult to assess the accuracy of noise prediction procedures." In this case, it is even difficult to specify the scatter of the data used in the correlations. This difficulty occurs for two reasons. First, the flap noise correlations are based on the results of numerous cold-flow and engine EBF tests which had varying degrees of data scatter depending on the configuration, test site, and method of reducing the data. Second, in correcting the data for ground effects, small but unknown errors in level were introduced while at the same time reducing the scatter in the original uncorrected data.

For these reasons only very rough estimates of the precision of the static flap noise prediction procedures can be made by the authors. It is considered that for both the UTW and OTW reference configurations the calculated OASPL levels in the flyover plane (except in the region within $\pm 15^{\circ}$ of the deflected exhaust direction) and in the wing-tip sideline direction ($\theta = 90^{\circ}$, $\varphi = 90^{\circ}$) will be accurate to within ±2 dB and SPL spectra should be accurate to within ±3.5 dB. Perceived noise level predictions are expected to be accurate to ±3 PNdB in the flyover plane and in the wing-tip sideline direction. The accuracy of these quantities when calculated for observer points at other azimuthal angles ($\varphi > 0$) is considered to be less. However, because of the complex three-dimensional acoustic field it is not possible at this time to give meaningful estimates of the precision of the predicted quantities.

PREDICTION OF AIRCRAFT MOTION EFFECTS ON FLAP NOISE

The 1/3-octave spectra obtained from the interim flap noise prediction procedure is for an aircraft which is stationary with respect to the observer. To complete the prediction procedure it is necessary to take into account forward velocity effects. No flight data for EBF aircraft were available to the authors, so that a prediction procedure for the effect of aircraft motion must necessarily rely on unverified analytical assumptions plus very limited data on relative airspeed effects from free jet (refs. 29, 53, 54, and 55) and wind tunnel data (refs. 10, 33, 51, and 52).

For these reasons, this part of the prediction procedure has been separated from the preceding sections. This permits the user the option of restricting his predictions to stationary aircraft or including an estimate of flight effects. Further, the separation of the procedures permits independent revision of either procedure.

In order to establish a preliminary procedure for predicting aircraft motion effects it will be assumed (as in refs. 54 and 55) that two independent processes are occurring which affect the flap noise.

(1) The effect of the relative motion of the dipole noise source with respect to the observer (dynamic amplification and Doppler frequency shift).

(2) Relative airspeed effects on the intensity of the dipole noise source.

The first effect can be estimated by assuming a dipole source is moving with respect to the observer at point O in figure 1. The dipole is moving through the atmosphere in the $\theta = 0^{o}$ direction at the aircraft velocity V_A, assuming that the engine angle of attack is zero. The convective (or dynamic) amplification (see refs. 56 and 57) caused by the relative motion of the source with respect to the observer O at angle θ (fig. 1) can be represented by

$$\Delta(\text{OASPL}) = -10\ \alpha_D \log\left(1 - \frac{V_A}{C_a}\cos\theta\right) \tag{20}$$

where $3 \leq \alpha_D \leq 4$. For a dipole source concentrated at a point, $\alpha_D = 4$. The Doppler frequency shift is

$$f_{FV} = \frac{f_C}{1 - \frac{V_A}{C_a}\cos\theta} \tag{21}$$

The relative airspeed effect on the source intensity can be obtained from data correlations based on recent unpublished Lewis Research Center acoustic tests with small UTW and OTW models immersed in a 13-inch diameter free-jet (described in refs. 29, 53, and 54) to simulate relative

airspeed effects. The test data in the flyover plane can be approximated by the following relation for typical take-off or landing velocities:

$$\Delta(\text{OASPL}) = 10 \log\left(\frac{V_E - V_A}{V_E}\right)^k \tag{22}$$

where V_E is the nozzle effective exhaust velocity. The empirical exponent k is a function of trailing flap angle ψ and observer angle θ; experimental values for the UTW case are given in figure 19 as a function of θ_F in the flyover plane. To use equation (22) in regions other than the flyover plane it must be assumed (because of lack of data) that k is independent of φ, so that at any φ, $k(\theta) = k(\theta_F)$. For the OTW case the airspeed effect was found to be negligible so that $k = 0$ is used. No systematic effect on frequency was observed for either the UTW or OTW models. Figure 19 shows that for the UTW case with a 60^o trailing edge angle the exponent k is 1.0 for angles between 0^o and 70^o, which is the region in which the dipole noise is maximum. At larger angles between $\theta = 80^o$ and 120^o the value of k increases rapidly because an increasing amount of quadrupole noise contaminates the dipole noise spectra.

The two processes can be combined into a single expression to represent the total aircraft motion effect on flap noise as follows

$$\text{OASPL}_{FV} = \text{OASPL}_\theta - 40 \log\left(1 - \frac{V_A}{C_a} \cos\theta\right) + 10\, k \log\left(\frac{V_E - V_A}{V_E}\right) \tag{23}$$

where α_D in equation (20) is arbitrarily assumed to be 4 (for a point source) and

$$f_{FV} = \frac{f_C}{1 - \frac{V_A}{C_a} \cos\theta} \tag{21}$$

RESEARCH REQUIREMENTS

The interim flap noise prediction procedures proposed herein for UTW and OTW EBF configurations have several serious shortcomings. First, the procedure is based primarily on correlations for the dipole-dominated region of the noise field. For angles close to the flap exhaust direction, $\theta = 180^{o} - (\psi \pm 30^{o})$, the intensified quadrupole noise emanating from the exhaust flowing adjacent to the flap system may dominate the spectra. This region usually shows a higher-order dependence on the exhaust velocity than does the dipole-dominated region. A separate prediction method needs to be developed for the quadrupole noise, so that it can be treated as a separate noise source distinct from the dipole source. The ultimate improvement would be to develop verified prediction methods for each of the important noise sources contributing to the flap noise field (similar to the general approach used in Ref. 37). The flap noise would then consist of the sum of these sources.

A second limitation is that the spectral shape presented herein does not vary continuously with θ and φ. In the flyover plane, for example, a single spectral shape is used for all θ_F. Thus, empirical equations are needed to more completely define the spectral shape and OASPL directivity as a function of θ and φ, or alternately, completely 1/3-octave-band SPL directivities must be specified in terms of θ and φ. To do this, much more complete three-dimensional flap noise experimental data (corrected to free field) are needed than are presently available to the authors. These improvements are particularly important for sideline noise predictions and footprint calculations.

A third and major weakness is in the prediction of flight effects on flap noise. In this area additional wind tunnel and free-jet experiments are needed along with tests to simulate the effects of source motion with respect to the observer. Ultimately, flight tests will have to be conducted with EBF aircraft (or simulated EBF aircraft).

A fourth weakness (which is major for the OTW case) is the lack of a definite method of predicting the effect of EBF configuration changes on the noise levels. Additional flap noise data are urgently needed for OTW

EBF configurations differing from the reference configuration of this report. Further, the noise scaling laws for OTW configurations need additional study and verification. For the UTW configuration, systematic studies of the effect on the flap noise field caused by varying the flap deflection angle and the position of the nozzle with respect to the wing-flap system are especially needed. Further, acoustic data on UTW EBF systems differing substantially from the reference configuration are needed to evaluate the sensitivity to major geometry changes. For example, no data are available for EBF models having very high bypass ratio nozzles to simulate engines with low pressure ratio fans (e.g., PR = 1.25). In addition, flap noise data for wings and flaps having shapes which differ considerably from the reference configuration are badly needed. The effects of surface acoustic treatment need further study and ultimately methods must be devised to include these effects on the predicted far field noise for a given configuration.

Finally, from a fundamental standpoint, the use of nozzle exit flow parameters to correlate the data is not considered the best choice for the UTW system. Ultimately an improved prediction procedure can be obtained by using the impingement parameter approach. However, this approach requires extensive analysis of engine exhaust plume data to obtain practical empirical equations for predicting flap impingement velocity radial profiles at the flap axial station. Further, a means of predicting the turbulence intensity profiles in the engine exhaust plume at the flap station must be developed.

CONCLUDING REMARKS

An interim method of predicting UTW and OTW externally blown flap noise has been presented. The procedure applies to configurations which have approximate geometric similarity to the reference configurations defined herein. The data correlations used are based primarily on Lewis Research Center in-house cold-flow model and contract engine (TF-34) test data.

It is intended that the proposed interim flap noise prediction procedure be periodically reviewed, revised, and upgraded. The data base used in

the correlations should be expanded to include flap noise data from other NASA centers and from airframe and engine manufacturers.

For the UTW prediction method it is recommended that the impingement parameter approach be used as soon as the necessary aerodynamic data becomes available. The impingement parameter approach, in addition to offering the promise of better accuracy, will permit the prediction of flap noise for UTW EBF systems employing high decay nozzles such as multi-lobed mixer nozzles. For the OTW case no practical alternative to the nozzle exit parameter approach can be suggested at this time.

Finally, it should be pointed out that the most accurate prediction of EBF noise for UTW configurations most likely can be made from an exact model of the configuration of interest. If careful measurements are made of the noise field, the results can be extrapolated to full scale by scaling the noise levels directly with nozzle area, and the frequency inversely with the diameter. Analysis of existing UTW data has shown that this scaling is quite precise. This approach of noise testing an exact model eliminates the data scatter introduced in the correlations of the generalized prediction method of this report, and also accounts for any significant configuration differences. This approach should also apply to OTW configurations when the noise scaling laws have been better substantiated.

During the preparation of this report, additional information has been published which was not used directly in the analyses of this report. For the convenience of the reader these are listed as references 58 to 70.

APPENDIX - SYMBOLS

A	area
BPR	mass-flow bypass ratio
C	speed of sound
D	nozzle diameter
d_i	characteristic impingement diameter
f	frequency, Hz
Δf	width of frequency band, Hz
I	turbulence intensity
K	geometry parameter (eqs. (10), (11), (16), (17), and (18))
k	exponent for relative airspeed effect (eq. (22))
O	observer position
OASPL	overall sound pressure level, ref. 20 N/m^2
P	pressure
p	sound pressure
R	distance to observer
SPL	sound pressure level, ref. 20 N/m^2
T	temperature
V	jet velocity
V_A	airspeed of aircraft
X, Y	horizontal and vertical position of nozzle (fig. 10)
α	pitch axis of engine axis with respect to ground plane
α_D	Doppler amplification exponent (eq. (20))
β	coefficient in Δ_φ directivity relation
Δ_{θ_F}	OASPL directivity with θ_F

Δ_φ OASPL directivity with φ

θ polar angle, engine inlet to observer position (fig. 1), deg

θ_F projection of polar angle θ on $\varphi = 0$ plane (fig. 1), deg

ρ density of air

φ azimuthal angle toward sideline (fig. 1), deg

ψ trailing flap angle (fig. 1), deg

Subscripts:

a ambient

C core

E effective

F fan (also see θ_F)

i impingement

N nozzle exit

o reference

p peak

REF reference value (eqs. (10) and (17))

STD standard day; 288.3 K (519° R); 101,035 N/m^2 (29.92 in. of Hg)

T total

Reference quantities:

A_o 0.093 m^2 (1.0 sq ft)

R_o 30.48 m (100 ft)

V_o 152.4 m/sec (500 ft/sec)

REFERENCES

1. Campbell, John P.; and Johnson, Joseph L., Jr.: Wind-Tunnel Investigation of an External-Flow Jet-Augmented Slotted Flap Suitable for Application to Airplanes With Pod-Mounted Jet Engines. NACA TN 3898, 1956.

2. Lowry, John G.; Reibe, John M.; and Campbell, John P.: The Jet-Augmented Flap. Preprint No. 715, S. M. Fairchild Fund Paper, Inst. of Aeronaut. Sci., Jan. 1957.

3. Turner, Thomas R.; Davenport, Edwin E.; and Riebe, John M.: Low-Speed Investigation of Blowing From Nacelles Mounted Inboard and on the Upper Surface of an Aspect-Ratio-7.0 35^{o} Swept Wing with Fuselage and Various Tail Arrangements. NASA MEMO 5-1-59L, 1959.

4. Maglieri, Domenic J.; and Hubbard, Harvey H.: Preliminary Measurements of the Noise Characteristics of Some Jet-Augmented-Flap Configurations, NASA MEMO 12-4-58L, 1959.

5. Dorsch, Robert G.; Krejsa, Eugene A.; and Olsen, William A.: Blown Flap Noise Research. AIAA Paper 71-745, June 1971.

6. Dorsch, Robert G.; Kreim, Walter J.; and Olsen, William A.: Externally-Blown-Flap Noise. AIAA Paper 72-129, Jan. 1972.

7. Olsen, William A.; Dorsch, Robert G.; and Miles, Jeffrey H.: Noise Produced by a Small-Scale Externally Blown Flap. NASA TN D-6636, 1972.

8. Gibson, Frederick W.: Noise Measurements of Model Jet-Augmented Lift Systems. NASA TN D-6710, 1972.

9. Putnam, Terrill W.; and Lasagna, Paul L.: Externally Blown Flap Impingement Noise. AIAA Paper 72-664, June 1972.

10. Falarski, Michael D.; Aoyagi, Kiyoshi; and Koenig, David G.: Acoustic Characteristics of Large-Scale STOL Models at Forward Speed. STOL Technology, NASA SP-320, 1972, pp. 443-454.

11. Lasagna, Paul L.; and Putnam, Terrill W.: Externally Blown Flap Impingement Noise. STOL Technology, NASA SP-320, 1972, pp. 427-433.

12. Jones, William L.; Heidelberg, Lawrence J.; and Goldman, Richard G.: Highly Noise Suppressed Bypass 6 Engine for STOL Applications. AIAA Paper 73-1031, Oct. 1973.

13. Samanich, Nick E.; Heidelberg, Lawrence J.; and Jones, William L.: Effect of Exhaust Nozzle Configuration on Aerodynamic and Acoustic Performance of an Externally Blown Flap System with a Quiet 6:1 Bypass Ratio Engine. AIAA Paper 73-1217, Nov. 1973.

14. Dorsch, Robert G.; Lasagna, Paul L.; Maglieri, Domenic L.; and Olsen, William A.: Flap Noise. Aircraft Engine Noise Reduction, NASA SP-311, 1972, pp. 259-290.

15. Olsen, William A.; Miles, Jeffrey H.; and Dorsch, Robert G.: Noise Generated by Impingement of a Jet Upon a Large Flat Board. NASA TN D-7075, 1972.

16. Dorsch, Robert G.; Goodykoontz, J. H.; and Sargent, Noel B.: Effect of Configuration Variation on Externally Blown Flap Noise. AIAA Paper 74-190, Jan.-Feb. 1974.

17. Hayden, Richard E.: Noise from Interaction of Flow with Rigid Surfaces. A Review of Current Status of Prediction Techniques. NASA CR-2126, 1972.

18. Clark, Bruce J.; Dorsch, Robert G.; and Reshotko, Meyer: Flap Noise Prediction Method for a Powered Lift System. AIAA Paper 73-1028, Oct. 1973.

19. Miles, Jeffrey H.: Rational Function Representation of Flap Noise Spectra Including Correction for Reflection Effects. AIAA Paper 74-193, Jan.-Feb. 1974.

20. Chestnutt, David; Maglieri, Domenic J.; and Hayden, Richard E.: Flap Noise Generation and Control. STOL Technology, NASA SP-320, 1972, pp. 413-426.

21. von Glahn, Uwe H.; Groesbeck, Donald E.; and Huff, Ronald G.: Peak Axial-Velocity Decay with Single- and Multi-Element Nozzles. AIAA Paper 72-48, Jan. 1972.

22. Goodykoontz, Jack H.; Olsen, William A.; and Dorsch, Robert G.: Small-Scale Tests of the Mixer Nozzle Concept for Reducing Blown-Flap Noise. NASA TM X-2638, 1972.

23. Goodykoontz, Jack H.; Dorsch, Robert G.; and Groesbeck, Donald E.: Noise Tests for a Mixer Nozzle - Externally Blown Flap System. NASA TN D-7236, 1973.

24. Goodykoontz, Jack H.; Dorsch, Robert G.; and Wagner, Jack M.: Acoustic Characteristics of Externally Blown Flap Systems with Mixer Nozzles, AIAA Paper 74-192, Jan.-Feb. 1974.

25. Hayden, Richard E., et al.: A Preliminary Evaluation of Noise Reduction Potential for the Upper Surface Blown Flap. (BBN-2473, Bolt, Beranek, and Newman, Inc.; NASI-11839.), NASA CR-112246, 1972.

26. McKinzie, Donald J., Jr.; and Burns, Robert J.: Externally Blown Flap Trailing Edge Noise Reduction by Slot Blowing. A Preliminary Study. AIAA Paper 73-245, Jan. 1973.

27. Reshotko, Meyer; Olsen, William A.; and Dorsch, Robert G.: Preliminary Noise Tests of the Engine-Over-the-Wing Concept. I. 30°-60° Flap Position. NASA TM X-68032, 1972.

28. Reshotko, Meyer; Olsen, William A.; and Dorsch, Robert G.: Preliminary Noise Tests of the Engine-Over-the-Wing Concept. II. 10°-20° Flap Position. NASA TM X-68104, 1972.

29. Dorsch, Robert G.; and Reshotko, Meyer: EBF Noise Tests with Engine Under-the-Wing and Over-the-Wing Configurations. STOL Technology, NASA SP-320, 1972, pp. 455-473.

30. Dorsch, Robert G.; Reshotko, Meyer; and Olsen, William A.: Flap Noise Measurements for STOL Configurations Using External Upper Surface Blowing. AIAA Paper 72-1203, Nov.-Dec. 1972.

31. von Glahn, Uwe H.; Reshotko, Meyer; and Dorsch, Robert G.: Acoustic Results Obtained with Upper-Surface-Blowing Lift-Augmentation Systems. Presented at the 84th Meeting of the Acoustical Society of America, Miami Beach, Fla., Nov. 28-Dec. 1, 1972. (NASA TM X-68159, 1972).

32. Reshotko, Meyer; Goodykoontz, Jack H.; and Dorsch, Robert G.: Engine-Over-the-Wing Research. AIAA Paper 73-631, July 1973.

33. Falarski, Michael D.; Aoyagi, Kiyoshi; and Koenig, David G.: Acoustic Characteristics of a Large-Scale Wind-Tunnel Model of an Upper-Surface Blown Flap Transport Having Two Engines. NASA TM X-62319, 1973.

34. Reshotko, Meyer; and Friedman, Robert: Acoustic Investigation of the Engine-Over-the-Wing Concept Using a D-Shaped Nozzle. AIAA Paper 73-1030, Oct. 1973.

35. Olsen, William A.; and Friedman, Robert: Noise Tests of the Engine-Over-the-Wing STOL Configuration Using a Multijet Nozzle with Deflector. NASA TM X-2871, 1973.

36. Karchmer, Allen M.; and Friedman, Robert: Noise Tests on an Externally Blown Flap with the Engine in Front of the Wing. NASA TM X-2942, 1973.

37. Guinn, Wiley A.; Blakney, Dennis F.; and Gibson, John S.: V/STOL Noise Prediction and Reduction. LG73ER0062, Lockheed Georgia Co. (FAA-RD-73-145), 1973.

38. Dunn, Daniel G.; and Peart, Noel A.: Aircraft Noise Source and Contour Estimation. (D6-60233, Boeing Commercial Airplane Co.; NAS2-6969.), NASA CR-114649, 1973.

39. Fink, Martin R.: Mechanisms of Externally Blown Flap Noise. AIAA Paper 73-1029, Oct. 1973.

40. Hayden, Richard E.: Fundamental Aspects of Noise Reduction from Powered-Lift Devices. SAE Paper 730376, Air Transportation Meeting, Miami, Florida, Apr. 1973.

41. Hersh, Alan S.; and Hayden, Richard E.: Aerodynamic Sound Radiation from Lifting Surfaces With and Without Leading-Edge Serrations. (Bolt, Beranek, and Newman, Inc.; NAS2-5974.), NASA CR-114370, 1971.

42. Curle, N.: The Influence of Solid Boundaries on Aerodynamic Sound. Proc. Roy. Soc. (London), Ser. A., vol. 231, No. 1187, Sept. 20, 1955, pp. 505-514.

43. Phillips, O. M.: On the Aerodynamic Sound from a Plane Turbulent Boundary Layer. Proc. Roy. Soc. (London), Ser. A., vol. 234, No. 1198, Feb. 21, 1956, pp. 327-335.

44. Powell, Alan: Aerodynamic Noise and the Plane Boundary. J. Acoust. Soc. Am., 32, No. 8, Aug. 1960, pp. 982-990.

45. Meecham, William C.: Surface and Volume Sound from Boundary Layers. J. Acoust. Soc. Am., vol. 37, No. 3, Mar. 1965, pp. 516-522.

46. Clark, P. J. F.; and Ribner, Herbert S.: Direct Correlation of Fluctuating Lift with Radiated Sound for an Airfoil in Turbulent Flow. J. Acoust. Soc. Am., vol. 46, No. 3, pt. 2, 1969, pp. 802-805.

47. Hersh, Alan S.; and Meecham, William C.: Sound Directivity Pattern Radiated by Small Airfoils. J. Acoust. Soc. Am., vol. 53, No. 2, Feb. 1973, pp. 602-606.

48. Charland, I. J.: Sources of Noise in Axial Flow Fans, J. Sound Vib., vol. 1, No. 3, 1964, pp. 302-322.

49. Vecchio, E. A.; and Wiley, C. A.: Noise Radiated from a Turbulent Boundary Layer. J. Acoust. Soc. Am., vol. 53, No. 2, Feb. 1973, pp. 596-601.

50. Patterson, R. W.; Amiet, R. K.; and Munch, C. L.: Isolated Airfoil-Tip Vortex Interaction. AIAA Paper 74-194, Jan.-Feb. 1974.

51. von Glahn, Uwe; Sekas, Nick; and Groesbeck, Donald: Forward Flight Effects on Mixer Nozzle Design and Noise Considerations for STOL Externally Blown Flap Systems. AIAA Paper 72-792, Aug. 1972.

52. Oetting, R. B.: Preliminary Wind Tunnel Noise Measurements of a Semi-Span Wing with an Upper-Surface Blown Flap. AIAA Paper 74-191, Jan.-Feb. 1974.

53. von Glahn, Uwe H.; Groesbeck, Donald; and Goodykoontz, Jack: Velocity Decay and Acoustic Characteristics of Various Nozzle Geometries with Forward Velocity. AIAA Paper 73-629, July 1973.

54. Dorsch, Robert G.: Externally Blown Flap Noise Research. SAE Paper 740468, Air Transportation Meeting, Dallas, Texas, May 1974.

55. Goodykoontz, Jack; von Glahn, Uwe H.; and Dorsch, Robert G.: Forward Velocity Effect on Under-the-Wing Externally Blown Flap Noise. AIAA Paper 75-476, Mar. 1975.

56. Lighthill, M. J.: Sound Generated Aerodynamically - The Bakerian Lecture 1961. Proc. Roy. Soc. (London), vol. 267A, 1962, pp. 147-182.

57. Lowson, Martin V.: The Sound Field for Singularities in Motion. Proc. Roy. Soc. (London), vol. 286A, no. 1407, 1965, pp. 559-572.

58. von Glahn, U. H.; and Groesbeck, D. E.: Influence of Mixer Nozzle Velocity Decay Characteristics on CTOL-OTW Jet Noise Shielding. AIAA Paper 75-97, 1975.

59. Heidelberg, L. H.; Homyak, L.; and Jones, W. L.: Full-Scale Upper-Surface-Blown Flap Noise. SAE Paper No. 750609, National Air Transportation Meeting, Hartford, Conn., May 6-8, 1975.

60. McKinzie, D. J.; and Burns, R. J.: Analysis of Noise Produced by Jet Impingement Near the Trailing Edge of a Flat and a Curved Plate. NASA TM X-3171, 1975.

61. Fink, M. R.: Investigation of Scrubbing and Impingement Noise. NASA CR-134762, 1975.

62. Cole, T. W.; and Rathbun, E. A.: Small Scale Model Static Acoustic Investigation of Hybrid High Lift Systems Combining Upper Surface Blowing with the Internally Blown Flap. NASA CR-114757, 1974.

63. Pennock, A. P.; Swift, G.; and Marbert, J. A.: Static and Wind Tunnel Model Tests for the Development of Externally Blown Flap Noise Reduction Techniques. NASA CR-134675, 1975.

64. Falarski, M. D.; Aiken, T. N.; Aoyagi, K.; and Koenig, D. G.: Comparison of the Acoustic Characteristics of Large-Scale Models of Several Propulsive-Lift Concepts. AIAA Paper 74-1094, 1974.

65. Bhat, W. V.; and Rosso, D. G.: Effect of Forward Speed on Jet Wing/Flap Interaction Noise. AIAA Paper 75-475, 1975.

66. Preisser, J. S.; and Fratello, D. J.: Acoustic Characteristics of a Large Upper-Surface Blown Configuration with Turbofan Engines. AIAA Paper 75-473, 1975.

67. Searle, N.: Acoustic Investigation of a Hybrid Propulsive Lift System, ASME Paper 74-WA/Aero-3, ASME Winter Annual Meeting, New York, Nov. 17-22, 1974.

68. Fink, M. R.: Scrubbing Noise of Externally Blown Flaps. AIAA Paper 75-469, 1975.

69. Fink, M. R.: Experimental Evaluation of Trailing Edge and Incidence Fluctuation Noise Theories. AIAA Paper 75-206, 1975.

70. Harkonen, D. L.; McBride, J. F.; and O'Keefe, J. V.: Noise and Static Performance Characteristics of a STOL Aircraft Jet Flap. NASA CR-137581, 1974.

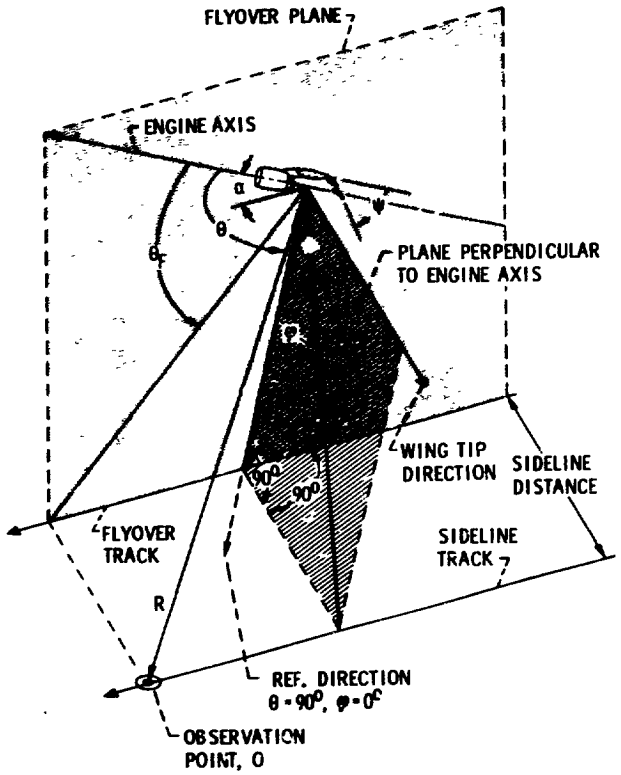

Figure 1 - Geometric variables describing flap noise field.

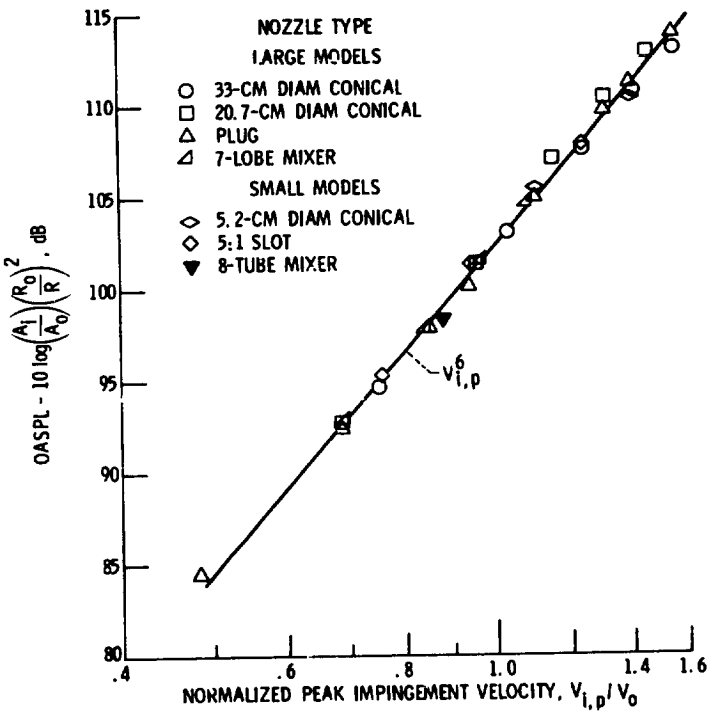

Figure 2. - Variation of flyover ($\varphi = 0$) radial peak value of normalized overall sound pressure level with impingement velocity for cold-flow two-flap UTW EBF configurations. Trailing flap angle, $\phi = 60^0$; $R_0 = 30.48$ m (100 ft); $A_0 = 0.093$ m^2 (1 ft^2); $V_0 = 152.4$ m/s (500 ft/sec).

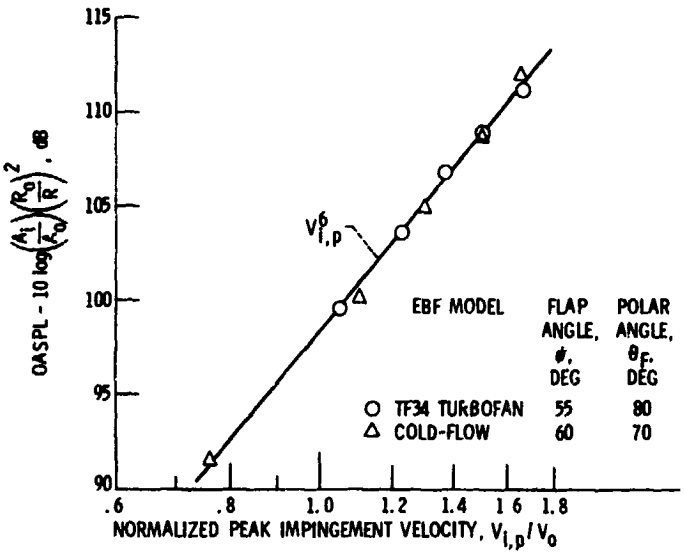

(a) NORMALIZED OASPL FOR POLAR ANGLE YIELDING THE FLY-OVER TRACK MAXIMUM.

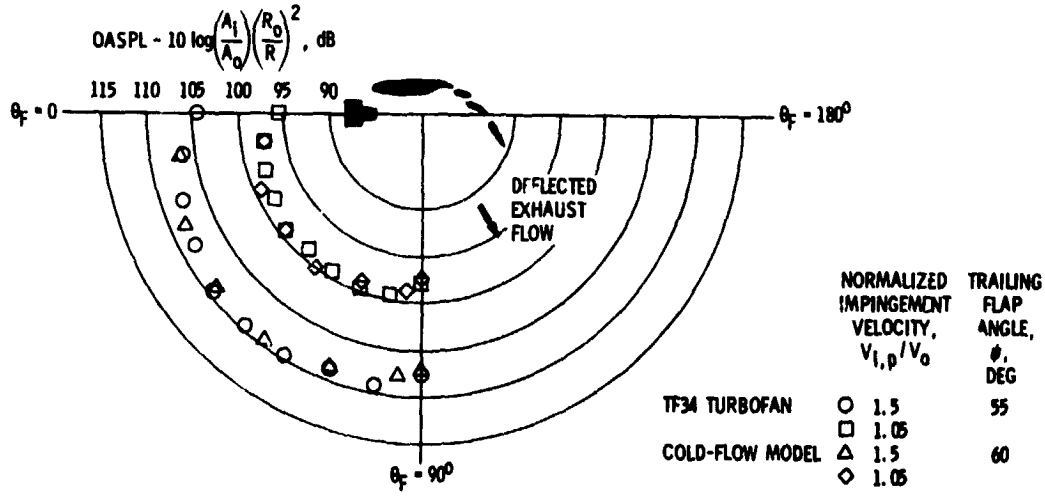

(b) FLAP NOISE DIRECTIVITY PATTERNS.

Figure 3. - Comparison of flap noise data in flyover plane (φ = 0) for turbofan engine and cold-flow coaxial-nozzle three-flap UTW test configurations using flap impingement flow parameters.

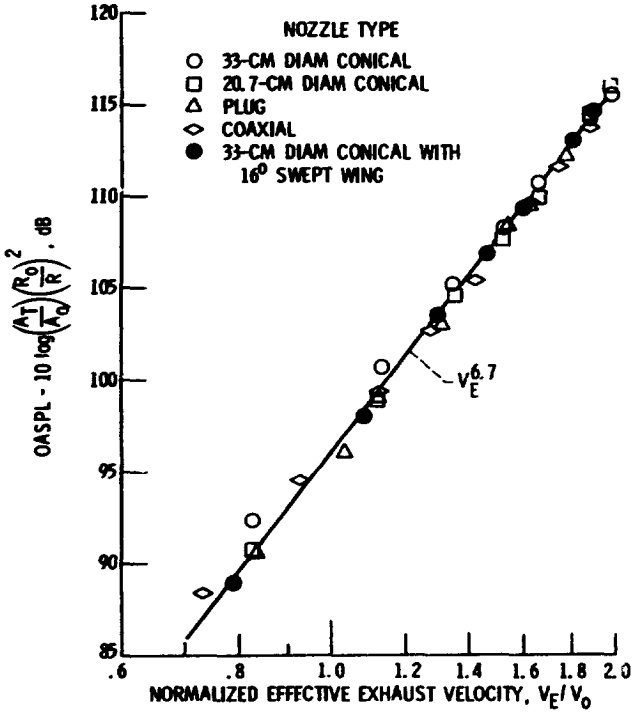

Figure 4. - Correlation of normalized overall sound pressure levels at angle of radial peak with effective nozzle exhaust velocity, for different cold-flow exhaust nozzles and two-flap EBF configurations. Flap angle, $\phi = 60^0$.

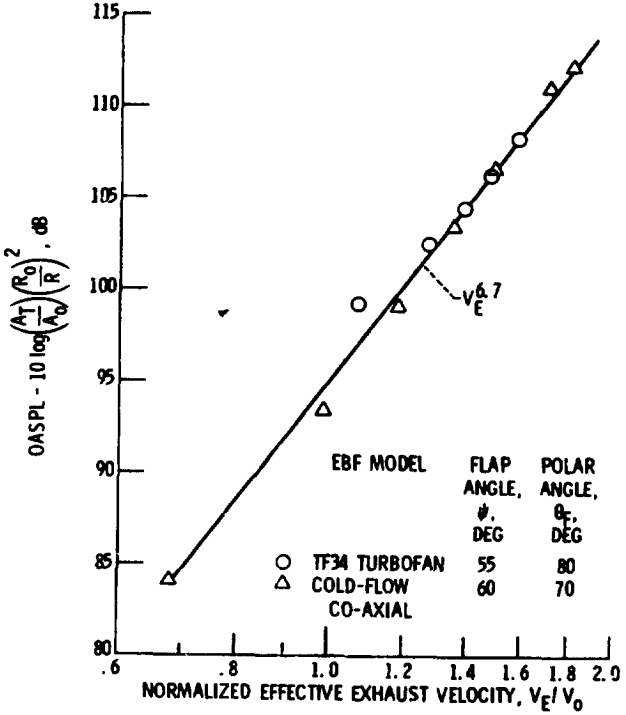

Figure 5. - Correlation of normalized overall sound pressure levels at angle of flyover maximum with effective nozzle exhaust velocity, comparing TF34 turbofan engine and cold-flow model results at large flap angles, ϕ.

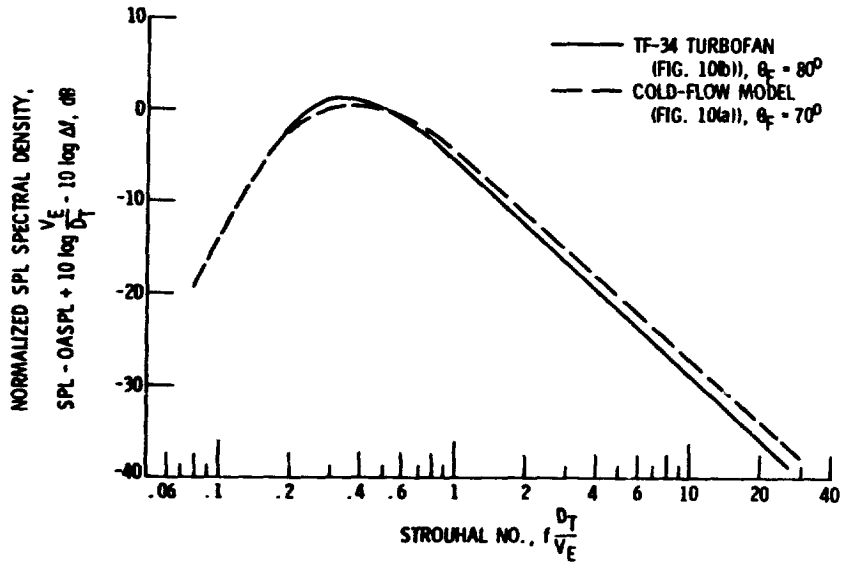

Figure 6. - Comparison of Strouhal correlations of flap noise spectral density for baseline TF-34 and cold-flow coaxial-nozzle model three-flap UTW EBF configurations. Trailing flap angle, 55° for TF-34 test and 60° for cold-flow model.

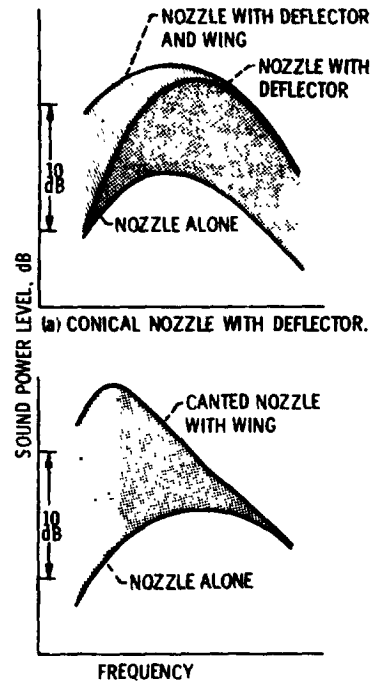

Figure 7. - Typical sound power level spectra for two types of OTW EBF systems.

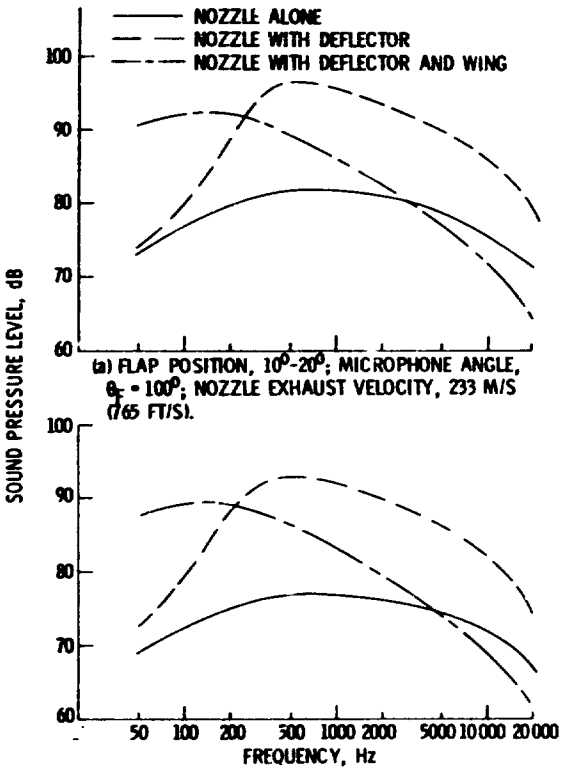

(a) FLAP POSITION, 10^0-20^0; MICROPHONE ANGLE, $\theta_F = 100^0$; NOZZLE EXHAUST VELOCITY, 233 M/S (765 FT/S).

(b) FLAP POSITION, 30^0-60^0; MICROPHONE ANGLE, $\theta_F = 80^0$; NOZZLE EXHAUST VELOCITY, 207 M/S (680 FT/S).

Figure 8. - Effect of high-frequency noise shielding by the wing for an OTW EBF system at angle, θ_F, of maximum flyover noise. Microphone distance is 15.2 m (50 ft). Smooth curves are drawn through ground effects in spectra.

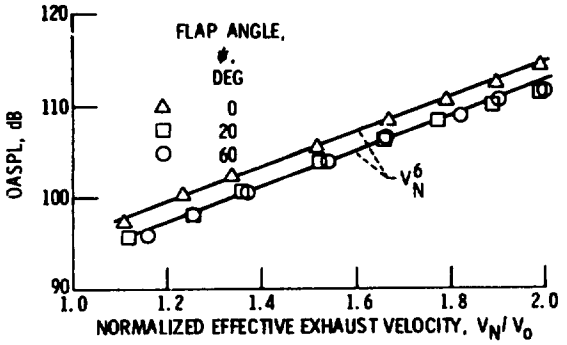

Figure 9. - Variation of overall sound pressure level at 15.2 m (50 ft) with nozzle exhaust velocity for large cold-flow OTW EBF model with conical nozzle and deflector. Microphone angle, $\theta_F = 90^0$.

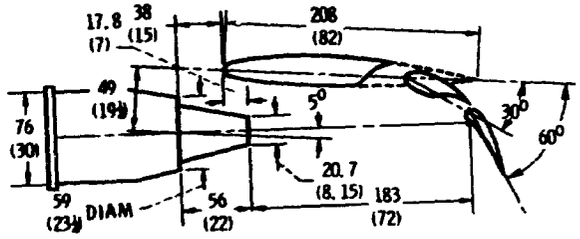

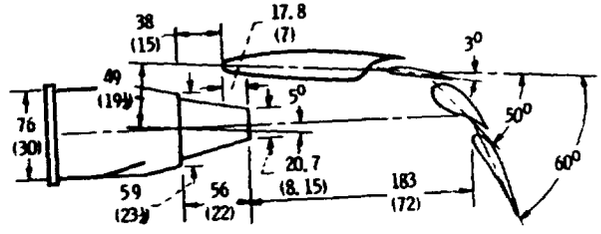

(a) BASELINE COLD-FLOW TWO AND THREE FLAP CONFIGURATIONS WITH COAXIAL NOZZLE. CORE EXHAUST AREA IS 334 CM^2 (51.8 $IN.^2$). ANNULAR EXHAUST AREA IS 1096 CM^2 (169.9 $IN.^2$).

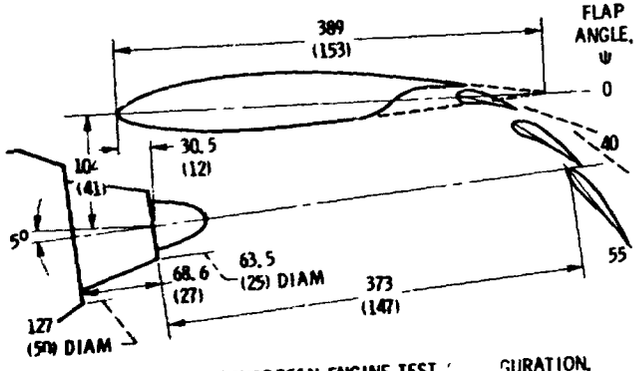

(b) BASELINE TF34 TURBOFAN ENGINE TEST CONFIGURATION. CORE EXHAUST AREA IS 1806 CM^2 (280 $IN.^2$). FAN EXHAUST AREA IS 5097 CM^2 (790 $IN.^2$).

Figure 10. - Reference UTW EBF configurations. Dimensions in centimeters (inches).

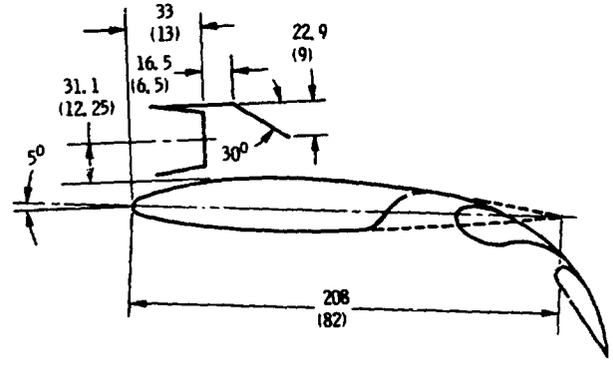

(a) BASELINE COLD-FLOW OTW CONFIGURATION. CONVERGENT NOZZLE DIAMETER 33 CM (13 IN.). FLAP SLOTS COVERED, 60° FLAP ANGLE SHOWN.

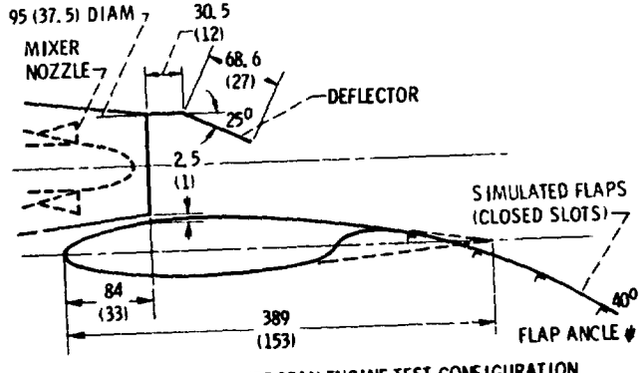

(b) BASELINE TF34 TURBOFAN ENGINE TEST CONFIGURATION. EXHAUST NOZZLE AREA IS 7123 CM^2 (1104 $IN.^2$).

Figure 11. - Reference OTW EBF configurations. Dimensions in centimeters (inches).

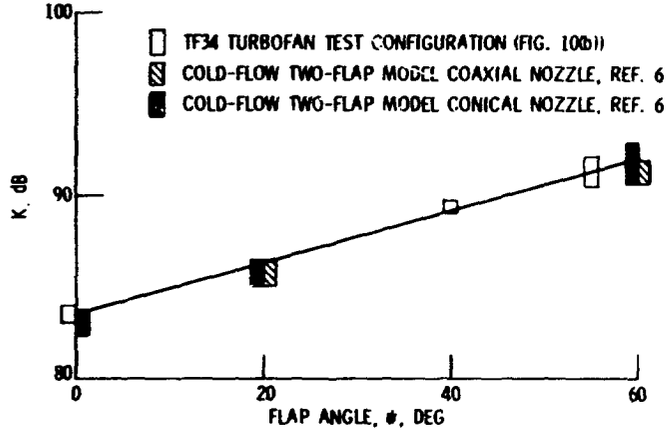

Figure 12. - Variation of K (eq. (11)) with flap angle for flap systems typical of configurations of figure 10(b) and reference 6. Scatter in K over the velocity range is indicated.

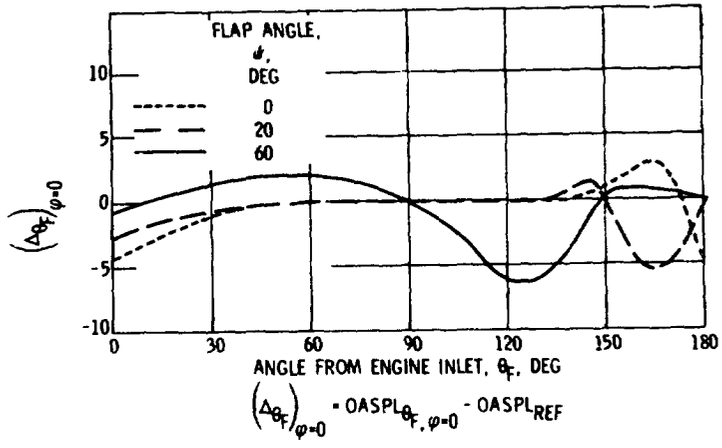

Figure 13. - Under-the-wing flap noise directivity at constant radius in the flyover plane ($\varphi = 0$).

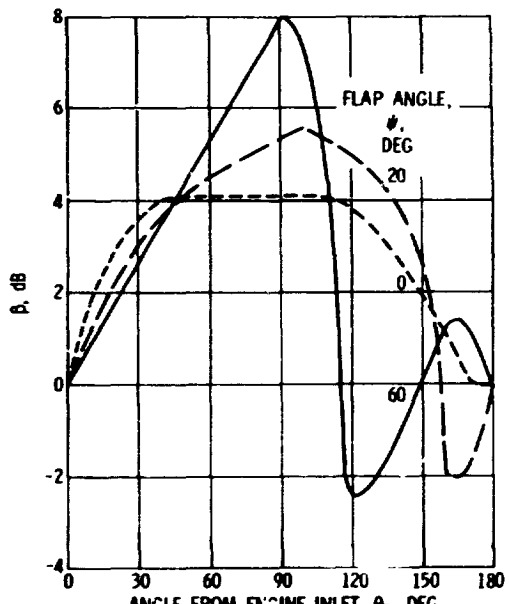

$$(\Delta_\varphi)_{\theta_F} = \beta(\cos\varphi - 1)$$

WHERE $(\Delta_\varphi)_{\theta_F} = OASPL_{\theta_F,\varphi} - OASPL_{\theta_F,\varphi=0}$

Figure 14. - Azimuthal OASPL directivity coefficient for UTW EBF noise at constant radius.

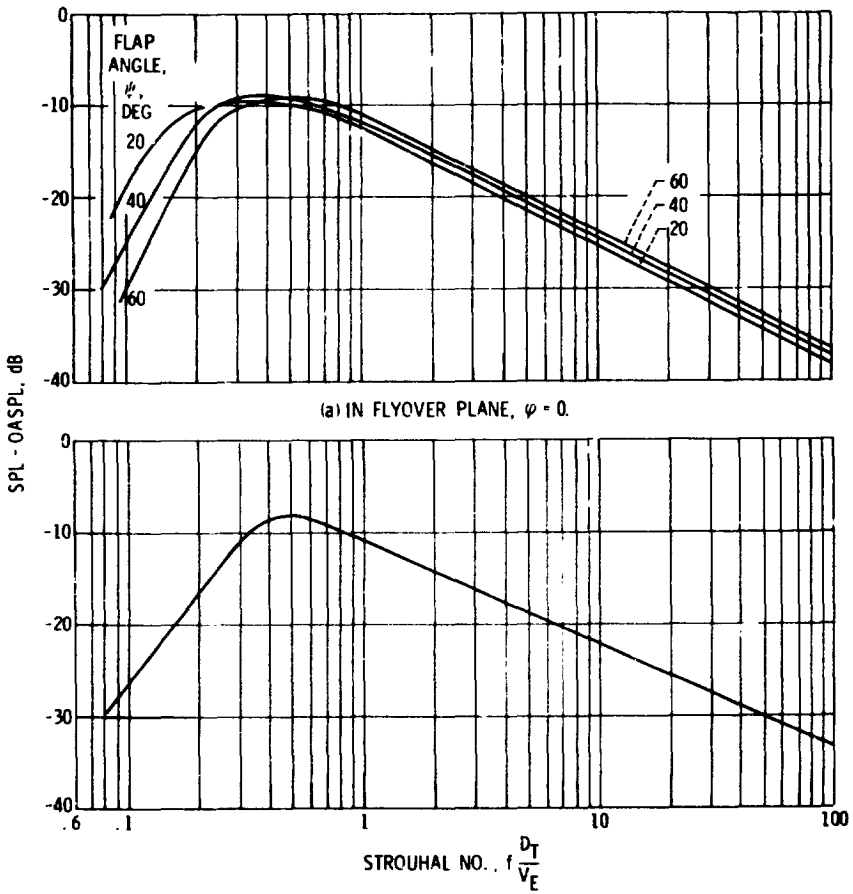

(a) IN FLYOVER PLANE, $\varphi = 0$.

(b) AT AZIMUTHAL ANGLE, $\varphi = 90^0$.

Figure 15. - Under-the-wing normalized flap noise spectra.

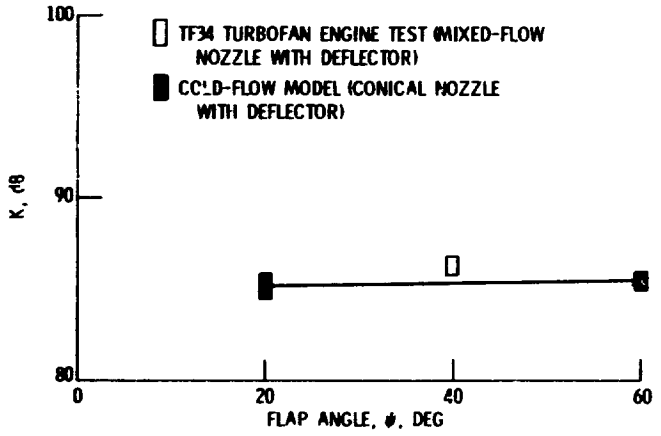

Figure 16. - Variation of K (eq. (18)) with flap angle for over-the-wing configurations. Scatter of measured values of K are shown.

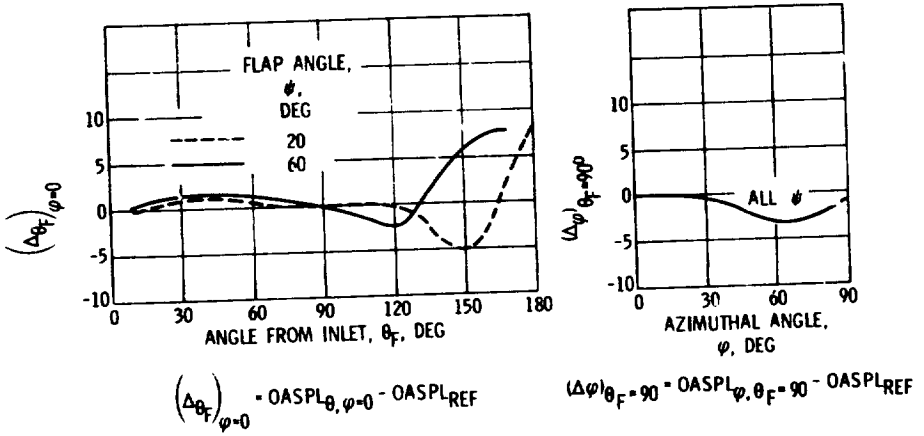

$$\left(\Delta_{\theta_F}\right)_{\varphi=0} = \text{OASPL}_{\theta,\varphi=0} - \text{OASPL}_{\text{REF}}$$

$$(\Delta\varphi)_{\theta_F=90} = \text{OASPL}_{\varphi,\theta_F=90} - \text{OASPL}_{\text{REF}}$$

(a) IN FLYOVER PLANE (φ = 0).

(b) IN PLANE PERPENDICULAR TO ENGINE AXIS ($\theta_F = 90^0$).

Figure 17. - Over-the-wing flap noise directivity at constant radius.

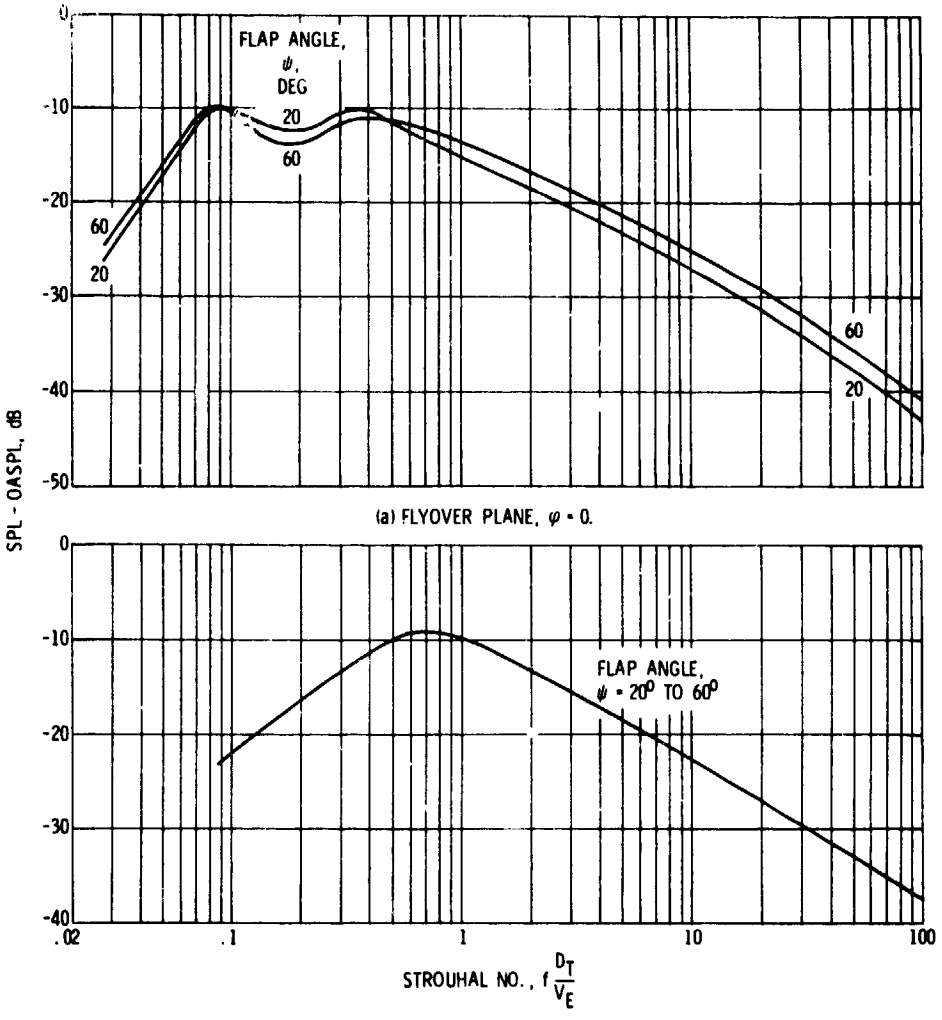

(a) FLYOVER PLANE, $\varphi = 0$.

(b) AT AZIMUTHAL ANGLE, $\varphi = 90^0$.

Figure 18. - Over-the-wing normalized flap noise spectra.

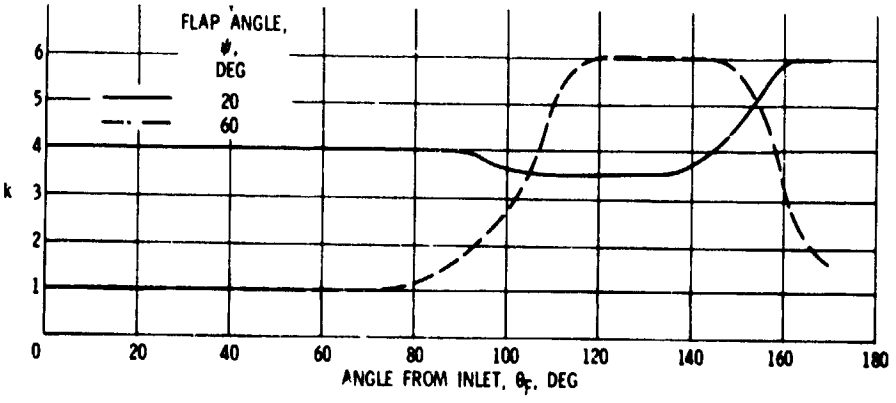

Figure 19. - Relative airspeed effect exponent, k, for UTW configurations. Flyover plane, $\varphi = 0$.